Renewable and Sustainable Energy Reviews 96 (2018) 502–525

Contents lists available at ScienceDirect

Renewable and Sustainable Energy Reviews

journal homepage: www.elsevier.com/locate/rser

A systematic review on CO_2 capture with ionic liquids: Current status and future prospects

Mahsa Aghaie, Nima Rezaei, Sohrab Zendehboudi*

Faculty of Engineering and Applied Science, Memorial University, St. John's, NL, Canada

ARTICLE INFO

Keywords:
CO_2 capture
Climate change
Absorption
Ionic liquids
Physical and thermodynamic properties

ABSTRACT

Global warming due to the emission of greenhouse gases, especially carbon dioxide (CO_2), has a significant effect on the climate change and has become a widespread concern in the recent years. Carbon capture, utilization, and sequestration (CCUS) strategy appears to be effective in decreasing the carbon dioxide level in the atmosphere. Despite a great progress in this field, there are still major limitations in commercialized the CO_2 capture methods that rely on absorption phenomena. High capital costs of for the CO_2 capture, low absorption and desorption rates (which require large facilities), solvent losses due to evaporation, and the use of corrosive solvents are among main obstructions. Recently, CO_2 capture with ionic liquids (ILs) has appreciably attracted researchers' attention. The distinct properties of ILs such as negligible vapor pressure and their affinity to capture the CO_2 molecules make them a feasible alternative for currently available solvents including, different amines.

This paper covers a brief review of previous engineering and research works on various CO_2 capture techniques, the description of CO_2 capture process using ILs, mechanisms of the CO_2 capture with ILs at molecular level, CO_2 and ILs properties, characterization of the CO_2/IL systems, impacts of operating and fluids conditions on CO_2 absorption capacity by ILs, and CO_2 solubility and selectivity in ILs. Moreover, the technical and economic aspects of the CO_2 capture with ILs, screening criteria for ILs/CO_2 systems, and important results obtained from previous studies will form the last parts of this manuscript. This review offers a proper/systematic guideline that assists researchers and engineers to comprehensively understand and to effectively design the CO_2/ILs processes, focusing on the thermodynamic and mass transfer aspects.

1. Introduction

It is believed that global warming is mainly resulted from the greenhouse gases (water vapor, carbon dioxide, methane, and nitrous oxide) which are trapping the heat in the Earth's atmosphere. Carbon dioxide (CO_2), which remains longer than other gases in the atmosphere, is more responsible for global warming and climate changes [1]. Carbon dioxide is naturally produced and consumed in the carbon cycle. As humans are currently consuming the long-buried carbons in the forms of fossil fuels and coal in significant amounts, excessive carbon is released in the atmosphere. On the other hand, the oceans (as a natural absorbent of CO_2) are not able to absorb all emitted carbon dioxide from the atmosphere [2].

Intergovernmental Panel on Climate Change (IPCC) report shows that about 79% of the total CO_2 emissions come from fossil fuels and minerals that are being used for power generation [3]. Coal power plants (operated by natural gas and oil) with 60% of the total CO_2 emissions have a great contribution to the global warming [3,4]. Hence, removing the carbon dioxide from flue-gases produced by power plants can effectively decrease the carbon level in the Earth's atmosphere. The production, processing, and utilization of fossil fuel sources such as oils, coals, and natural gases undoubtedly will continue. Thus, it seems necessary to use them as clean as feasible through employing effective strategies for carbon and other pollutants reduction. Carbon capture, utilization, and storage (CCUS) is an emerging method which helps to better manage CO_2 concentration through various ways such as capturing carbon, sequestration, or/and turning it to useful chemicals [4,5].

Carbon capture processes, in general, are divided into three main categories including pre-combustion, post-combustion, and oxy-combustion. In the post-combustion and oxy-combustion methods, the fuel is burned with air and oxygen, respectively. The heat released in these methods is used to generate electricity. The main difference between the post-combustion and oxy-combustion processes is the composition of the flue-gas. In the latter technique, the flue-gas contains highly concentrated CO_2, which seems suitable for underground storage.

* Corresponding author.
E-mail addresses: szendehboudi@mun.ca, sohrab.zendehboudi@gmail.com (S. Zendehboudi).

https://doi.org/10.1016/j.rser.2018.07.004
Received 30 December 2017; Received in revised form 18 March 2018; Accepted 1 July 2018
Available online 29 August 2018
1364-0321/ © 2018 Elsevier Ltd. All rights reserved.

Nomenclatures

Acronyms

AAD	average absolute deviation
AIL	aprotic ionic liquid
ANN	artificial neural network
CILs	conventional ionic liquids
CC	capital cost
CCS	carbon capture and storage
CCUS	carbon capture, utilization, and storage
DE	differential evolution
DESs	deep eutectic solvents
DETL	differential evolution with Tabu List
EOS	equation of state
GA	genetic algorithm
GHG	greenhouse gas
HBDs	hydrogen bond donors
IGCC	integrated gasification combined cycle
IL	ionic liquid
IPCC	Intergovernmental Panel on Climate Change
IUPAC	International Union of Pure and Applied Chemistry
LLE	liquid-liquid equilibria
LM	Levenberg-Marquart
MD	molecular dynamics
MOFs	metal-organic frameworks
NRTL	non-random two liquid equation of state
OC	operating cost
OME	operating and maintenance expenses
PC-SAFT	perturbed chain statistical association fluid theory
PILs	protic ILs
PR	Peng-Robinson equation of state
PT	Patel-Teja
PRSV	Peng-Robinson-Stryjek-Vera equation of state
PSO	particle swarm optimization
RK	Redlich-Kwong equation of state
SA	simulated annealing
SAFT	statistical association fluid theory
SRK	Soave-Redlich-Kwong equation of state
TGA	thermogravimetric analysis
TSIL	task-specific ionic liquid
vdW	van der Waals
VL	van Laar equation of state
VLE	vapor-liquid equilibria
WS	Wong-Sandler mixing rule

Chemicals

AMP	2-amino-2-methl-1-propanol
BF_4^-	tetra fluoroborate anion
[bmim][BF_4]	1-butyl-3-methylimidazolium tetrafluoroborate
[bmim] [Br]	1-butyl-3-methylimidazolium bromide
[bmim] [dca]	1-butyl-3-methylimidazolium dicyanamid
[bmim][NO_3]	1-butyl-3- methylimidazolium nitrate
[bmim][NTf_2]	1-butyl-3-methylimidazolium bis(trifluorome thylsulfonyl)imide
[bmim][CF_3SO_3]	1-butyl-3-methylimidazolium trifluorome thanesulfonate
[bmim][PF_6]	1-butyl-3-methylimidazolium hexafluorophosphate
[bmim][TfO]	1-butyl-3-methylimidazolium trifluorome thanesulfonate
Br^-	bromide anion
CF_3-$CFH_2CH_3SO_3^-$	methylsulfate anion
[$CH_3CH_2NH_3$][NO_3]	ethylammonium nitrate
CO_2	carbon dioxide
CO_3^{2-}	carbonate
[C_2Mpyrr][Br]	1-ethyl-1-methylpyrrolidinium bromide
[C_nC_nMIM]$^+$	1-alkyl-3-alkylimidazolium cation (n = carbon chain length)
[C_nMIM]$^+$	1-alkyl-3-methylimidazolium cation (n = carbon chain length)
[C_2mim][NTf_2]	1-ethyl-3-methylimidazolium bis(trifluorome thylsulfonyl)imide
[emim][$EtSO_4$]	1-ethyl-3-methylimidazolium ethyl sulfate
[emim][TfO]	1-ethyl-3-methylimidazolium trifluorome thanesulfonate
HCO_3^-	bicarbonate
Hg	mercury
hmg	hexamethylguanidinium
[hmim][BF_4]	1-hexyl-3-methylimidazolium tetrafluoro borat
[hmim] [Ntf_2]	1-hexyl-3-methylimidazolium trifluorome thanesulfonate
[hmim][PF_6]	1-hexyl-3-methylimidazolium hexafluoro phosphate
HSO_4^-	hydrogen sulfate anion
MDEA	methyl diethanolamine
MEA	monoethanolamine
[N-bupy][BF_4]	*N*-butylpyridinium tetrafluoroborate
$N(CN)^{2-}$	dicyanamide anion
N4111	tetrabutylammonium
NaCl	sodium chloride
$N_{n,n,n,n}^+$	tetraalkylammonium cation (n = carbon chain length)
NO_2	nitrogen dioxide
NPf^{2-}	bis(pentafluoroethylsulfonyl)imide anion
O_2	oxygen
OAc^-	acetate anion
omim	1-octyl-3-methyl imidazolium
[omim][BF_4]	1-methyl-3-octylimidazolium tetrafluoroborate
[omim][Cl]	1-octyl-3-methylimidazolium chloride
PDMS	polydimethylsiloxane
$[PF_6]^-$	hexafluorophosphate
pmg	pentamethylguanidinium
PP	polypropylene
ppg	pentamethylpropylguanidinium
PPO	polyphenyleneoxide
[P_{14666}][2-CNpyr]	trihexyl(tetradecyl)phosphonium 2-cyanopyrrolide
[P_{14666}][3-CF_3pyra]	trihexyl(tetradecyl)phosphonium 3-(trifluoromethyl) pyrazolide
[P_{14666}][Br]	trihexyl(tetradecyl)phosphonium bromide
[P_{14666}][Cl]	trihexyl(tetradecyl)phosphonium chloride
[P_{14666}][Gly]	trihexyl(tetradecyl)phosphonium glycinate
[P_{14666}][Ile]	trihexyl(tetradecyl)phosphonium isoleucinate
$P_{n,n,n,n}^+$	tetraalkylphosphonium cation (n = carbon chain length)
[$Py_{n,n}$]+	1-alkyl-1-alkylpyrrolidinium cation (n = carbon chain length)
[Rmim][Tf2N]	1-alkyl-3-methylimidazolium (alkyl = methyl, butyl, octyl, and dodecyl) bis(trifluoromethylsulfonyl)imides
SCN^-	thiocyanate anion
SO_2	sulphur dioxide
tba	tetrabutylammonium

[TBMA][Cl]	tributylmethylammonium chloride
tbp	tetrabutylphosphonium
tea	tetraethylammonium
tma	tetramethylammonium
tmg	tetramethylguanidinium
ttp	trihexyl(tetradecyl)phosphonium

Variables/Parameters

A	Antoine constant in Eq. (6); viscosity model coefficient in Eq. (10)
A_J, A_L, A_M	critical temperature model constants in Eqs. (11), (14) and (18), respectively
a	constant in Eq. (11); constant in vapor pressure model in Eq. (25); energy parameter in Eqs. (33), (A.1), (A.7), (A.8), and Table A.1
a_1, a_2, and a_3	constants in dentistry-temperature correlation in Eq. (8)
a_c	a constant in energy parameter in Eq. (30)
a_i, and a_j	a coefficient in reduced effective cross section model in Eq. (3); energy parameter for component i and j in Eqs. (A.1), (A.3), (A.6), (A.7), (A.8), (A.12), (A.14) and Table A.1
a_{ij}	attractive forces between molecules i and j in Eqs. (A.3), (A.12), (A.14), and Table A.1
$\tilde{\alpha}$	Helmholtz free energy in Eqs. (32) and (33)
$\tilde{\alpha}^{assoc}$	association contribution of Helmholtz free energy in Eq. (32)
$\tilde{\alpha}^{disp}$	dispersion contribution of Helmholtz free energy in Eq. (32)
$\tilde{\alpha}^{hc}$	hard chain molecules contribution of Helmholtz free energy in Eq. (32)
B	coefficient of vapor pressure model in Eqs. (6) and (23); parameter in density model in Eqs. (7) and (9)
b	coefficient in vapor pressure model in Eq. (25); volume parameter in Eqs. (28), (31), (A.5), (A.6), (A.7), (A.9) and in Tables 6, 7, and A.1
b_1 and b_2	volume parameter for component i and j in Eqs. (A.2), (A.4), (A.5), (A.9), (A.13), (A.15) and Table A.1
b_i and b_j	volume parameter for component i and j in Eqs. (A.2), (A.4), (A.5), (A.9), (A.13), (A.15) and Table A.1
b_{ij}	binary interaction coefficient of molecules i and j in Eqs. (A.2), (A.4), (A.6), (A.13), (A.15) and Table A.1
C	coefficient of vapor pressure model in Eq. (6); coefficient in density model in Eq. (7); parameter in Eq. (A.6), Eq. (A.7), and Table A.1
C_J, C_L, C_M	critical pressure model constants in Eqs. (12), (15), and (19), respectively
C_p	specific heat capacity at constant pressure in Eq. (25)
c	volume parameter in Tables 6, 7
D_J	parameter in critical pressure model in Eq. (15)
d_{ij}	parameter in viscosity-temperature model in Eq. (5)
E_J, E_L, E_M	critical volume model constants in Eqs. (13), (16) and (20), respectively
f_2	fugacity of component 2 (solute) in Eqs. (35), (36), (A.10), and (A.11)
G^E	Gibbs excess free energy in Eq. (A.6), Eq. (A.7), and Table A.1
H_2	enthalpy of component 2 (solute) in Eqs. (35) and (A.10)
I_{ji}	binary interaction coefficient between molecules j and i in Eq. (A.8) and Table A.1
k	transmission coefficient in Eq. (24)
k_1	coefficient in energy parameter model in Table 8
k_{ij}	binary interaction coefficient in Eqs. (A.1), (A.3), (A.4), (A.7), (A.14) and in Table A.1
K_{ij}'	binary interaction coefficient in Eq. (A.15)
M	molecular weight in Eqs. (19), (24), and (26)
M_{ref}	molecular weight of sample in Eq. (27)
M_S	molecular weight of sample in Eq. (27)
m	mass in Eqs. (24) and (26)
m_{ref}	mass of reference in Eq. (27)
m_S	mass of sample in Eq. (27)
N	number of atoms in molecule in Eq. (15)
n_i	number of occurrences of group i in Eqs. (11)–(20)
n_{pts}	number of data points in Eq. (34)
P	pressure
P_b	bubble point pressure
P_c	critical pressure
P_{Ji}, P_{Li}, P_{Mi}	contributions of component i to critical pressure in Eqs. (12), (15), and (19), respectively
P^{sat}	saturation pressure
R	universal gas constant
S	orifice area in Eq. (24)
S'	surface area to liquid in Eq. (24)
T	temperature
T^*	reduced temperature in Eqs. (2)–(5)
T_b	boiling point temperature
T_c	critical temperature
T_{Ji}, T_{Li}, T_{Mi}	contributions of component i to critical temperature in Eqs. (12), (14), and (18), respectively
T_r	reduced temperature
t	time in Eqs. (26) and (27)
u	parameter in PRSV model in Table 6
V	volume
V_c	critical volume
V_{Ji}, V_{Li}, V_{Mi}	contributions of component i to critical volume in Eqs. (13), (16), and (20), respectively
v	parameter in PRSV model in Table 6
V_2^{∞}	partial molar volume of solute at infinite dilatation in Eqs. (35) and (A.10)
w	parameter in PRSV model in Table 6
x_i and x_j	mole fraction of component i and j, respectively

Greek Letters

α	vaporization coefficient in Eqs. (24) and (26); energy parameter in Eq. (29) and Table 7
Δ	change or difference
ϕ	fugacity coefficient
$\sigma_\mu^*(T^*)$	reduced effective cross section in Eqs. (2) and (3)
δ	parameter in five parameter EOSs in Eq. (28) and Table 7
ε	particle energy in Eq. (4); activation energy in Eq. (10); a parameter in five parameter EOS in Eq. (28) and Table 7
η	apparent viscosity in Eq. (10); a parameter in five parameter EOS in Eq. (28) and Table 7
κ	conductivity in Table 4
ρ	density
τ	elapsed time in Eq. (24)
ω	acentric factor

Subscripts and Superscripts			
		E	excess
		exp	experiment
0	reference state, and dilute	hc	hard chain
*	reduced	LV	liquid-vapor
∞	infinite dilution	m	melting
assoc	association	r	reduced
b	boiling	ref	reference
c	critical	res	residual
calc	calculation	s	sample
disp	dispersion	sat	saturation

However, in the post-combustion method, further stages/process units are required to capture the carbon from the flue-gas [6].

The pre-combustion method is associated with the integrated gasification combined cycle (IGCC). In the pre-combustion, the fuel is gasified to produce syngas [7]. The syngas, which contains CO and H_2, is utilized as a feed for the water-gas-shift reactors. In the presence of steam, CO is converted to CO_2 and H_2. CO_2 is then captured from the outlet stream and H_2 is combusted to generate the energy. Post-combustion is easier to be implemented as a retrofit option in the existing power plants, compared to other two approaches [6]. In other words, pre-combustion and oxy-combustion methods can only be applied in new power plants [8].

As illustrated in Fig. 1, the post-combustion carbon capture technique is divided into several main subcategories such as absorption, microbial (algal), adsorption, membrane, and cryogenics. Among these techniques, absorption is more popular and is widely employed in the commercial post-combustion CO_2 capture plants. In this method, the flue-gas in the tall columns or towers (known as absorbers) is in contact with the solvent, which captures CO_2 from the flue-gas. The rate of CO_2 absorption with solvent is a crucial parameter in the chemical absorption processes. High absorption rate not only can reduce the capital costs of CO_2 capturing, but is also considered as an asset for an absorption process to be operated at the industrial scale [9,10]. Fig. 2 also illustrates a simple schematic of CO_2 absorption and desorption columns in a typical carbon capture plant.

Various solvents in the chemical absorption of CO_2 capture processes have been introduced [13]. Amines due to their high reactivity with CO_2 molecules, high thermal stability, and high absorption capacity are widely used as the absorbent for carbon capture operations [14]. Among all amine groups, monoethanolamine (MEA), tertiary amines such as methyl diethanolamine (MDEA), and sterically hindered amines such as 2-amino-2-methl-1-propanol (AMP) are the common absorbents for CO_2 capture systems [15]. Application of amines faces several drawbacks; including, high construction cost, high equipment corrosion rate, and amine degradation by SO_2, NO_2, and O_2 in the flue-gases which induces a high absorbent make-up rate and high energy

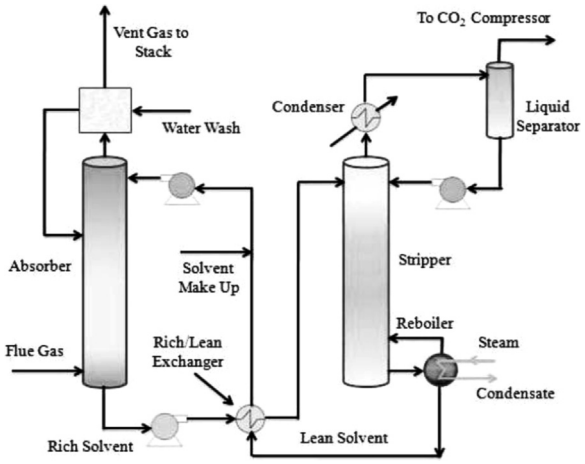

Fig. 2. Schematic figure of absorption/desorption columns in a CO_2 capture process (modified after [12]).

Table 1
General properties of ionic liquids [19].

Property	General characters
Salt ions	large cations and anions
Freezing temperature	< 100 °C
Liquidous temperature	> 200 °C
Thermal stability	high
Viscosity	< 100 cP, workable
Dielectric constant	< 30
Polarity	moderate
Specific conductivity	< 10 mS/cm, good
Vapor pressure	negligible
Solvency	strong
Catalytical character	excellent (for organic reactions)

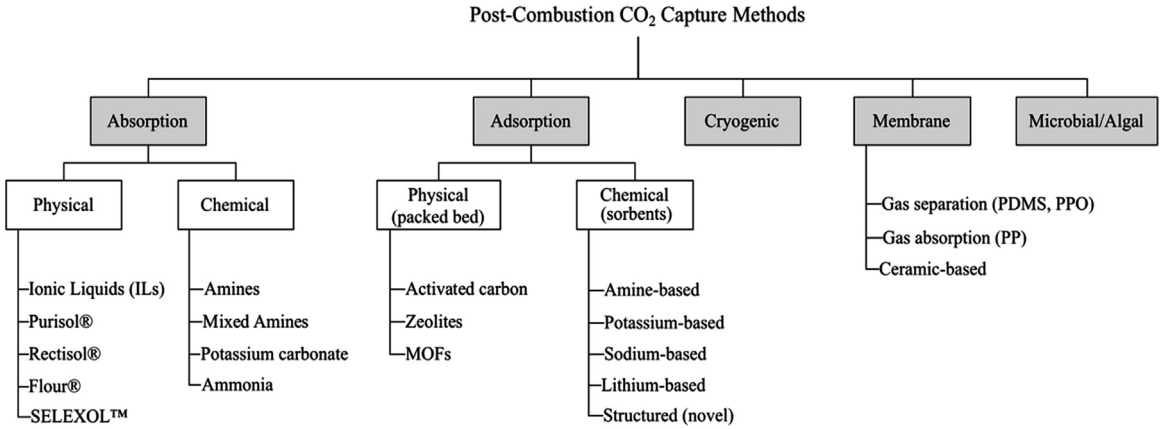

Fig. 1. Diagram of main carbon separation/capture methods in the post-combustion category (modified after [11]). [MOFs: metal-organic frameworks; PDMS: polydimethylsiloxane; PPO: polyphenyleneoxide; PP: polypropylene].

consumption during high-temperature absorbent regeneration processes where large equipment are required [16]. These disadvantages are linked with the inherent properties of amines, which have high vapor pressures, corrosive nature, and high energy inputs for regeneration [17]. Several research studies have been conducted to replace amines with superior solvents, which have lower volatility, better thermal stability, lower corrosive characteristic, lower degradation rate, and lower regeneration cost [12–15]. Recently, ionic liquids (ILs) have been proposed as a potential replacement solvent for amines in the carbon capture processes [18]. The general properties of a majority of ILs are listed in Table 1 [19].

Strong ion-ion interactions for ILs (compared to other common intermolecular forces such as London forces and ion-dipole interactions in organic solvents) lead to negligible evaporation at the ambient conditions [20]. Other appealing properties of ILs are their high thermal stability, large electrochemical window, and their ability to dissolve compounds with various polarities [21]. Furthermore, physical and chemical properties of ILs can be adjusted by altering the cation and anion parts to make them suitable for particular applications [22]. From the environmental point of view, ILs are inflammable, non-volatile, and recyclable which make them environmentally friendly, compared to other chemicals such as amines [23,24].

In a research work, Blanchard et al. [25] reported that CO_2 gas can be considerably dissolved into the certain ILs. Since then, there is a growing interest in exploring and understanding the solubility of various gases in ILs [13,22,23].

A drawback to use ILs for CO_2 capture is their high viscosity due to their complex synthesis and purification processes. ILs have higher viscosity, compared to conventional solvents [26]. This character makes them less suitable for industrial CO_2 capture since the rate, at which the CO_2 is absorbed by ILs, is much slower. Solvents that have a lower viscosity tend to be more favorable for this separation purpose as the pumping costs are lower and the mass transfer rates are normally higher [27]. According to Krupiczka et al. [28], the viscosity of ILs can be modified by using a proper combination of cations and anions. The cation has generally a lower impact on ILs properties than the anion. With increasing the alkyl chain of cations, the viscosity of ILs increases. The effect of anion on viscosity in imidazolium based ILs is reported as $[bmim][NTf_2] < [bmim][CF_3SO_3] < [bmim][BF_4] < [bmim][PF_6]$. The viscosity of ILs also changes by adding a co-solvent. The effect of co-solvent in decreasing viscosity depends on the solvent polarity and the extent of dissociation of ILs into ions. Polar solvents such as water lower the viscosity more than nonpolar solvents; including, benzene and toluene. For instance, the role of water in reducing the viscosity of hydrophobic ILs is prominent.

Conventional ILs capture the carbon through a physical absorption mechanism. Although adjusting cations/anions in the ILs can enhance the solubility of CO_2 in conventional ILs, compared to the current commercial carbon capture technologies such as amine-based solvents, their CO_2 capture capacity is still low [29]. A comprehensive understanding of molecular structure/interactions and accurate determination of thermodynamic and physical characters such as solubility, vapor-liquid equilibria (VLE), liquid-liquid equilibria (LLE), selectivity, density, and viscosity are necessary to employ appropriate ILs in different applications/cases. To use ILs in gas separation processes, it is required to understand the phase behavior of ILs/gas systems. A well-developed methodology to obtain phase equilibrium conditions is thermodynamic modeling using appropriate equations of state (EOSs). A large number of research works have focused on the solubility of gases in common imidazolium-based ILs with $[BF4]^-$ and $[PF_6]^-$ anions [26–28]. Karakastani et al. [30] predicted the solubility of CO_2 in some ILs through employing perturbed chain-statistical associating fluid theory (PC-SAFT) EOS where they considered the quadrupole interactions between CO_2 molecules, dipolar interactions between ionic liquid (IL) molecules, and the Lewis acid-base type of association between the IL and the CO_2. They found a great agreement between the modeling results and experimental data at pressures 0–100 MPa. Shiftlet et al. [31,32] utilized the most popular EOSs including Redlich–Kwong (RK), Soave-Redlich-Kwong (SRK), van der Waals (vdW), and Peng-Robinson (PR) with proper mixing rules for multi-component mixtures. They concluded that the experimental solubility data of CO_2, SO_2, CF_3-CFH_2, and NH_3 in ILs are well correlated with the cubic (modified) EOSs. Andrew et al. [33] examined Soft-SAFT EOS ability to estimate the solubility of CO_2 in $[C_n\text{-mim}][NTf_2]$ using one binary parameter, resulting in a good match with the experimental data. Chen et al. [6] checked the competence of PC-SAFT with and without associating parameters in determining the solubility of CO_2 in imidazolium based ILs where the temperature-dependent binary interaction parameters were taken into account. The results revealed that PC-SAFT is able to acceptably forecast the solubility so that the modeling results were very close to the real data. It was also found that PC-SAFT with the associating parameters describes VLE more precise, compared to that without the associating parameters.

The solubility of gases in ILs can be increased by extending the interface area of gas/ILs systems and by increasing the operating pressure. Maginn et al. [18] examined the solubility of nine different gases into $[bmim][PF_6]$ IL and found out that water and CO_2 have strong interactions. CO_2 in ILs exhibits higher solubility, compared to solubility of ethylene, ethane, methane, carbon monoxide, hydrogen, and nitrogen in ILs. Argon and oxygen have also very low solubility in ILs. They also reported Henry's law constants of gases in ILs. The gas solubility can be explained based on the molecules interactions in terms of polarizability and dipole and quadrupole moments between the gas and solvent molecules. It should be noted that the mixing enthalpy and entropy can also indicate the strength of interactions between CO_2 and ILs. Yokozeki et al. [34] successfully correlated the experimental solubility of CO_2 in 18 ILs to fluids properties and operating conditions through using Redlich-Kwong equation of state (RK-EOS). In addition, they presented the data in terms of excess functions (excess Gibbs free energy, G^E; excess enthalpy, H^E; and excess entropy, S^E). Depending on the magnitudes of these excess functions, the CO_2 absorption might be a chemical or physical process.

The thermodynamic behaviors of CO_2/ILs systems such as physical and chemical properties, phase equilibrium of CO_2/ILs mixtures, and solubility and selectivity of CO_2 in ILs should be properly investigated. A suitable equation of state (EOS) and mixing rules are required to accurately model the thermodynamic behaviors of CO_2 and IL systems. A part of the common EOSs for research investigations in this area are PR EOS, RK EOS [35], SRK EOS [36], Predictive Peng-Robinson EOS, Peng-Robinson-Stryjek-Vera EOS, Sanchez-Lacombe EOS [37], PC-SAFT EOS, extended PC-SAFT (PC-PSAFT) EOS, and truncated PC-PSAFT EOS [38]. The solubility of CO_2 in most of ILs is not determined yet, since a majority of the previous studies have assessed the solubility of CO_2 in common imidazolium based ILs [5,14,30]. Thus, modified versions of various EOSs need to be utilized to obtain the solubility of CO_2 in phosphonium, pyridinium, ammonium, and guanidinium based ILs.

In this review paper, CO_2 capture using ILs is briefly described in terms of mechanisms, advantages, and disadvantages. The past research works in this research field are discussed and their main findings are reported. Comprehensive information on the properties and thermodynamic behaviors of CO_2, ILs, and CO_2 / ILs systems is also provided. The last sections summarize the practical, economic, and theoretical aspects of CO_2 capture with ILs.

2. CO_2 emissions: sources and statistical data

Global greenhouse gas (GHG) emissions are mainly due to human activities, including fossil fuel burning, deforestation, and industrial processes. Among different sources of GHG emissions, the energy sector has the largest contribution [39,40]. The other shares come from agriculture, industrial processes, and solid biomass burning for generation of heat and energy. Due to economic growth and population

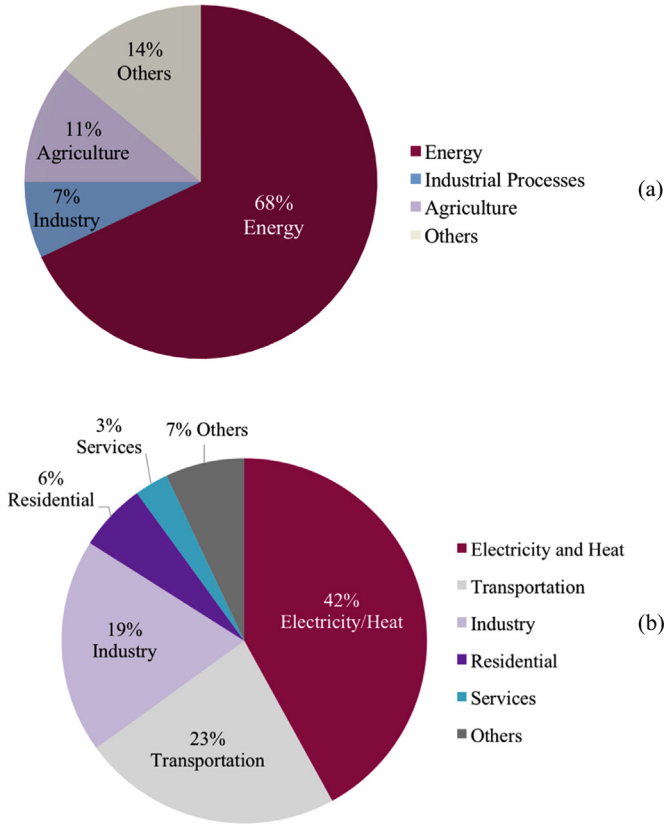

Fig. 3. Schematic plot of: (a) shares of global anthropogenic GHG emissions and (b) world CO_2 emissions from fuel combustion by sector in 2014 (modified after [40]).

increase, the energy demand is increasing. Global total primary energy supply has increased by 150% from 1971 to 2014 [39]. CO_2 has the largest share of the anthropogenic GHG emissions. The growing world energy demand is mainly responsible for increasing the CO_2 emissions. In 2014, global CO_2 emissions reached 32.4 Gt CO_2, of which 82% comes from energy sector, mainly due to burning of fossil fuels. Among the fossil fuels, 34% is from oil, 46% from coal, 19% from gas fuels, and the remaining 1% has been resulted from nuclear, hydro, geothermal, solar, wind, biofuels, and waste [39]. Global GHG emissions from various sectors and world CO_2 emissions from fuel combustion are

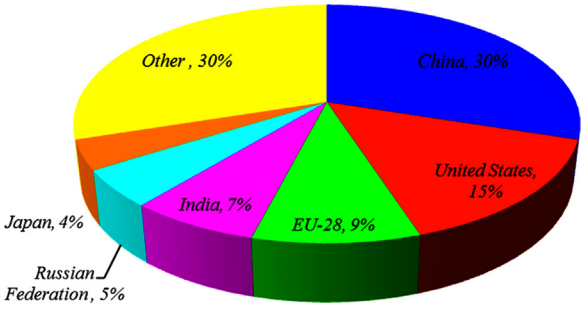

Fig. 5. Regional distribution of 2014 global CO_2 emissions from fossil fuels combustion and industrial processes (modified after [45]).

depicted in Fig. 3(a) and Fig. 3(b), respectively [40]. Electricity and heat generation, and transportation together are two major sectors, producing about two-third of the global CO_2 emissions from fuel combustion. A significant extent of the GHG emissions in heat and electricity generation is from coal, while the road transportation is responsible for most of the CO_2 emissions in transportation sector.

In the atmosphere, the average volume concentration of CO_2 is about 385 ppm (or, 582 ppm by mass); the total mass of CO_2 in the atmosphere is therefore about 3.0×10^{15} kg [36,37]. The concentration of CO_2 varies by season, geographical region, and human-induced activities that produce carbon [41]. Fig. 4 demonstrates the CO_2 emissions by sectors in the period of 1971–2014 [40,42]. According to Fig. 4, the global carbon emissions from fossil fuels have been increased by about 90% since 1971. The carbon emissions from all sectors have exhibited a considerable increase from 1971 to 2014. In 2016, the annual rate of CO_2 emissions increased from 3.2 ppm at the beginning of 2016 to 3.6 ppm towards the end [43].

Total carbon dioxide emitted by region in 2014 is illustrated in Fig. 5. China has the highest contribution to the CO_2 emissions. It is clear that increasing the atmospheric carbon dioxide (CO_2) concentration will lead to an increase in CO_2 concentration in the ocean surface, because of the gas exchange between the air and oceans. Hence, the dissolved inorganic carbon (e.g., CO_2, HCO_3^-, and CO_3^{2-}) will be increased and subsequently the pH of the ocean surface will decrease, resulting in the ocean acidification [44].

3. CO_2 properties

Carbon dioxide (CO_2) is an odorless and colorless gas at the atmospheric condition. This chemical component is relatively nontoxic,

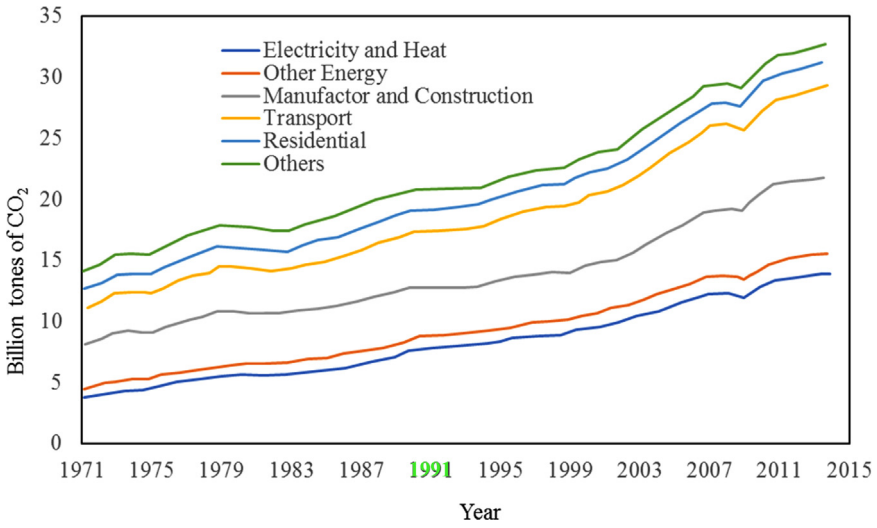

Fig. 4. Global CO_2 emissions by sector in the period 1971–2014 (modified after [40,42]).

noncombustible, and soluble in water. Its molecular weight is 44.009 g/mol. Normal melting point of CO_2 is −56.5 °C and its solubility in water is 2.9 g/L at 25 °C [46]. CO_2 is also miscible with hydrocarbons and organic liquids at particular thermodynamic conditions [57,58]. The density of gas CO_2 is 1.976 g/l at 25 °C. Its vapor pressure and viscosity are 5720 kPa (56.5 atm) at 20 °C and 0.01503 cP at the atmospheric condition, respectively [47]. The surface tension of CO_2 is 0.0162 N/m at the melting point [58].

3.1. Viscosity

The viscosity of CO_2 in other conditions can be calculated using Eq. (1), where it expresses $\mu(\rho, T)$ as a summation of three terms. The first term $\mu_0(T)$ is the dilute gas viscosity at a given temperature, $\Delta\mu(\rho, T)$ is the excess viscosity which signifies the effect of density (or pressure), and $\Delta\mu_c(\rho, T)$ is the critical enhancement due to fluctuations near the critical point [48]. Eq. (1) represents the above description in the mathematical form:

$$\mu(\rho, T) = \mu_0(T) + \Delta\mu(\rho, T) + \Delta\mu_c(\rho, T) \tag{1}$$

Fenghour et al. [49] proposed the following correlation to calculate the viscosity of carbon dioxide in dilute regions:

$$\mu_0(T) = \frac{1.00697T^{1/2}}{\sigma_\mu^*(T^*)} \tag{2}$$

where $\mu_0(T)$ is the zero-density viscosity in $\mu Pa.\ s$, T is the temperature in Kelvin, and $\sigma_\mu^*(T^*)$ denotes the reduced effective cross section, which is represented by the following empirical equation:

$$\ln \sigma_\mu^*(T^*) = \sum_{i=0}^{4} a_i (\ln T^*)^i \tag{3}$$

The reduced temperature (T^*) can be calculated using the following expression:

$$T^* = \frac{kT}{\varepsilon} \tag{4}$$

where ε is the particle energy, k stands for the Boltzmann constant, and T represents the absolute temperature ($\frac{\varepsilon}{k} = 251.196\ K$). a_i is a coefficient in Eq. (3) which is listed in Table 2.

The excess viscosity describes the viscosity behavior change with the density outside the critical region as given by the following expression:

$$\Delta\mu(\rho, T) = \sum_{i=1}^{n} b_i(T)\rho^i \ \text{ where } \ b_i = \sum_{j=1}^{m} \frac{d_{ij}}{T^{*(j-1)}} \tag{5}$$

where T^* stands for the reduced temperature as defined by Eq. (4) and d_{ij} denotes a coefficient, which is obtained through curve fitting of the excess viscosity experimental data versus the reduced temperature.

3.2. Vapor pressure

The vapor pressure (P^{sat}) of CO_2 can be calculated using the Antoine equation as follows [50]:

$$\log P^{sat}(\text{mmHg}) = A - \frac{B}{C + T(^{\circ}\text{C})} \tag{6}$$

where A, B, and C are the constants (For CO_2: $A = 9.8206$, $B = 1347.790$, and $C = 273.00$) [50].

3.3. Thermodynamic behavior and critical properties

Fig. 6 presents the pressure-temperature diagram of CO_2. As depicted in Fig. 6, the triple point represents the temperature and pressure (− 56.7 °C and 5.11 atm) that three phases can coexist at the thermodynamic equilibrium. The critical point of CO_2 corresponds to 73.8 atm and 31.1 °C [51,52].

To reasonably forecast the thermodynamic behavior of any component or mixture through using equations of state (EOSs), the critical properties and acentric factor of the component/mixture are required. The critical properties and acentric factor of CO_2 are listed in Table 3 [52].

4. Ionic liquids (ILs) characteristics

Based on the molecular structure, ILs are classified into proton-donating (protic ILs (PILs)) and nonproton-donating (aprotic ILs (AILs)) solvents. A general structure of cations and anions in ILs molecular configuration is shown in Fig. 7.

In Table 4, the characteristics of ILs are listed and compared to the atomic, molecular, and molten salts. As clear from Table 4, ILs due to their various structures and ions have different solvent properties, compared to the atomic salts; however, they are similar to the polar protic liquids and molten salts in terms of physical characteristics.

4.1. Density

ILs are denser than water, except pyrrolidinium dicyano-diamide and guanidinium with a density ranging from 0.90 g/cm^3 to 0.97 g/cm^3. As shown in Fig. 8, the density of ILs declines while the number of carbons in the alkyl chain increases. Furthermore, the density of 1-methylimidazolium ILs decreases linearly with increasing temperature. An increase in the viscosity value of ILs is noticed with increasing the number of carbons in the alkyl group, which exhibits a different trend, compared to the viscosity behavior for conventional organic solvents. High viscosity of ILs is attributed to the van der Waals interactions and hydrogen bonding. Generally, the molecular interactions increase with alkyl lengthening or/and fluorination.

Luciana Tome et al. [54] showed that experimental density data of ILs are in good agreement with the Tait equation [55] for density of liquids which is given below.

$$\rho = \frac{\rho(T, P = 0.1MPa)}{\left[1 - C \ln \frac{(B + P)}{(B + 0.1)}\right]} \tag{7}$$

$$\rho(T, P = 0.1MPa) = a_1 + a_2 T + a_3 T^2 \tag{8}$$

$$B = b_1 + \frac{b_2}{T} \tag{9}$$

where a_1, a_2, and a_3 can be fitted to the experimental density data for different ILs versus temperature. C, b_1, and b_2 are also obtained if the density is plotted against temperature and pressure, using Eqs. (7)–(9).

4.2. Viscosity

The empirical equation for the apparent dynamic viscosity (η in cP) of ILs to describe its temperature dependency is as follows [56]:

$$\eta = A\ e^{\varepsilon/RT} \tag{10}$$

where A represents a constant for a given liquid, ε is the activation energy for viscous flow of liquid, T is the temperature in Kelvin, and R

Table 2
Coefficients used in Eq. (3) to obtain viscosity of CO_2 at low density [49].

i	a_i
0	0.235156
1	− 0.491266
2	5.211155×10^{-2}
3	5.347906×10^{-2}
4	-1.537102×10^{-2}

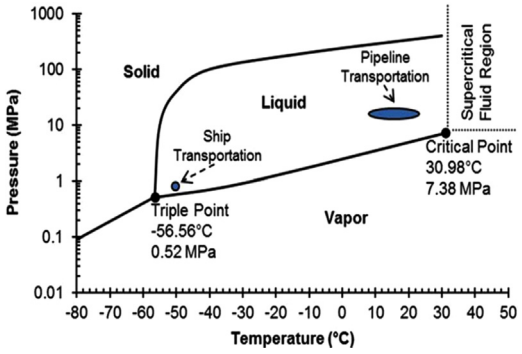

Fig. 6. CO_2 phase diagram (reprinted with permission from [51]).

Table 3
Critical properties of CO_2 [52].

Critical parameter	Designation/symbol	Value
Temperature	T_c (K)	304.2
Pressure	P_c (bar)	73.8
Volume	V_c ($cm^3\ mol^{-1}$)	94.0
Acentric factor	ω	0.2236

denotes the universal gas constant in J/(mol K). Temperature and chemical additives strongly affect the viscosity of ILs. For instance, increasing temperature or/and adding organic solvents lead to a reduction in the viscosity.

The surface tension data of ILs is rare in the literature. It has been reported that ILs have a higher surface tension than conventional solvents (e.g., hexane with a surface tension of 1.8 Pa.cm); but, not as much as water (7.3 Pa.cm) [57]. For instance, the surface tensions of most imidazolium based ILs at 298.15 K are in the range of 2.5 (Pa.cm) to 3.5 (Pa.cm).

4.3. Critical properties

The critical properties of ILs are not readily available and should be estimated due to the decomposition phenomenon at temperatures near the boiling point. There are certain techniques/methods introduced by researchers to determine the critical properties of ILs. For instance, Valderrama and Robles [58] employed an extended group contribution method based on the concepts developed by Lydersen [59] and Joback and Reid [60] to obtain the critical properties, normal boiling points, and acentric factors of ILs. In this method, only structure of the ILs and their molecular weights are required [61]. It is accurate enough to be used in the generalized correlations and methods based on equations of state. The absolute average deviation (AAD) of calculated and experimental liquid densities is 5–6% [61]. The critical properties and acentric factors for some common ILs are tabulated in Table 5.

The group contribution method for estimation of critical properties was developed by Lydersen [59]. In this approach, the critical properties of a compound are calculated based on the contribution of certain groups of atoms and the number of frequency of group of atoms in a molecule, through using the following expressions:

$$T_c = \frac{T_b}{A_L + \sum n_i \Delta T_{Li} - (\sum n_i \Delta T_{Li})^2} \tag{11}$$

$$P_c = \frac{M}{[C_L + \sum n_i \Delta P_{Li}]^2} \tag{12}$$

$$V_c = E_L + \sum n_i \Delta V_{Li} \tag{13}$$

in which, n_i stands for the number of times that a group appears in the molecule, T_b represents the normal boiling temperature, ΔT_{Li} denotes the contribution of group i to the critical temperature, ΔP_{Li} symbolizes the contribution of group i to the critical pressure, ΔV_{Li} is the contribution of group i to the critical volume, M is the molecular weight, and A_L, C_L, and E_L are the constants equal to 0.567, 0.34, and 40, respectively [59]. Eqs. (14)–(16) were also proposed by Joback and Reid [60] to determine the critical properties:

$$T_c = \frac{T_b}{A_J + \sum n_i \Delta T_{Ji} - (\sum n_i \Delta T_{Ji})^2} \tag{14}$$

$$P_c = \frac{1}{[C_J + D_J N - \sum n_i \Delta P_{Ji}]^2} \tag{15}$$

$$V_c = E_J + \sum n_i \Delta V_{Ji} \tag{16}$$

where N is the number of atoms in the molecule and A_J, B_J, C_J, D_J, and E_L represent the constants which are equal to 0.584, 0.965, 0.113, 0.0032, and 17.5, respectively [60].

The combination of Lydersen's method, Joback Reid method, and

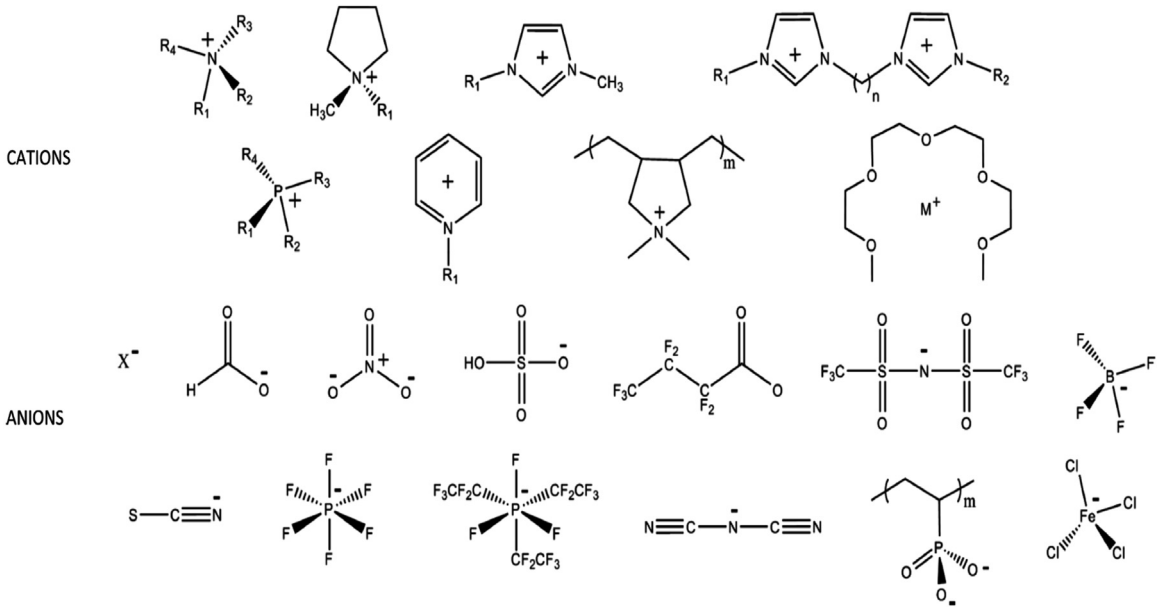

Fig. 7. Structures of cations and anions of most common ionic liquids [53].

Table 4
A comparison between the physical properties of different solvents [53].

Parameter[a]	Solvent type				
	Atomic	Molecular	Molten salt	Ionic liquid	
	Hg	H_2O	NaCl	PIL $[CH_3CH_2NH_3]$ $[NO_3]$	AIL $[C_4mim]$ $[PF_6]$
T_m (°C)	-38.8	0	801	12	10
T_b (°C)	356.7	100	1413	255	409
ρ (g/cm^3)	13.53	0.997	1.539	1.21	1.366
μ (Pa.s)	1.526×10^{-3}	8.95×10^{-4}	12.5×10^{-4}	35.9×10^{-4}	36.9×10^{-4}
P^{sat} (Pa)	2.67	3173	12700	0.49	$<10^{-2}$
$D\times10^{-6}$ (cm^2/s)	85	22.99	Na^+: 80.1 Cl^-: 63.5	$[CH_3CH_2NH_3^+]$: 0.158 $[NO_3^-]$: 0.151	$[C_4mim^+]$: 1.5 $[PF_6^-]$: 1.8
γ_{LV} (mN/m)	486.5	72.8	111.7	47.3	43.8
κ (S/cm)	10^5	5.5×10^{-4}	0.256	2.69×10^{-2}	1.4×10^{-3}
Cp (J/mol.K)	27.98	75.3	66.9	206	406

[a] T_m: melting temperature; T_b: boiling temperature; ρ: density; μ: viscosity; P^{sat}: vapor pressure; D: diffusion coefficient; γ_{LV}: interfacial tension of liquid-vapor; κ: conductivity; and Cp: specific heat capacity at constant pressure.

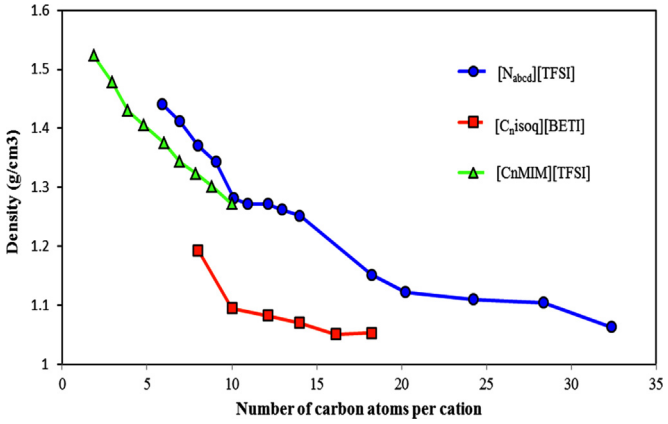

Fig. 8. Density variation of ILs with number of carbons [21].

the technique proposed by Alvarez and Valderrama [63] was resulted in a proper strategy, called "modified Lydersen-Joback-Reid" method, as presented by the following equations:

$$T_b = 198.2 + \sum n_i \ \Delta T_{bMi} \tag{17}$$

$$T_c = \frac{T_b}{A_M + \sum n_i \Delta T_{Mi} - (\sum n_i \Delta T_{Mi})^2} \tag{18}$$

$$P_c = \frac{M}{[C_M + \sum n_i \Delta P_{Mi}]^2} \tag{19}$$

$$V_c = E_M + \sum n_i \Delta V_{Mi} \tag{20}$$

The constant parameters in Eqs. (18)–(20) are $A_M = 0.5703$, $B_M = 1.0121$, $C_M = 0.2573$, and $E_M = 6.75$ [58].

Valderrama et al. [58] extended the "modified Lydersen-Joback-Reid method" to ILs. Following this strategy, the acentric factor is calculated using Eq. (21):

$$\omega = \frac{(T_b - 43)(T_c - 43)}{(T_c - T_b)(0.7T_c - 43)} \log\left(\frac{P_c}{P_b}\right) - \frac{(T_c - 43)}{(T_c - T_b)} \log\left(\frac{P_c}{P_b}\right) + \log\left(\frac{P_c}{P_b}\right) - 1 \tag{21}$$

Valderrama et al. [64] used the group contribution method with 44 defined groups and prepared the most complete database for the critical properties of ILs.

4.4. Vapor pressure

The vapor pressure of chemical components is required in many applications such as separation, solvent selection, and design and operation of process equipment. According to the literature, ILs have a negligible vapor pressure. There are a few models to predict the vapor pressure of ILs.

The vapor pressure of ILs might be estimated through the equilibrium condition concept, implying the same fugacity of each component in both vapor and liquid phases [65].

The vapor pressure of ILs can also be calculated using the Antoine equation ($\log P^{Sat} = A - B/(T + C)$) with water as a reference (C = 43). Valderrama and Sanga [62] suggested Eqs. (22) and (23) to determine

Table 5
The critical properties of common imidazolium based ionic liquids [58,62].

IL	IUPAC Name[a]	T_c (K)	P_c (bar)	V_c (cm^3/mol)	ω
[bmim][PF6]	1-*n*-butyl-3-methylimidazolium hexafluorophosphate	708.9	17.3	779.5	0.7553
[hmim][PF6]	1-hexyl-3-methylimidazolium hexafluorophosphate	754.3	15.5	893.7	0.8352
[bmim][BF4]	1-butyl-3-methylimidazolium tetrafluoroborate	623.3	20.4	672.0	0.8489
[hmim][BF4]	1-hexyl-3-methylimidazolium tetrafluoroborat	679.1	17.9	786.2	0.9258
[N-bupy][BF4]	*N*-butylpyridinium tetrafluoroborate	597.6	20.3	648.1	0.8307
[omim][Cl]	1-octyl-3-methylimidazolium chloride	860.1	20.3	814.2	0.6190
[emim][EtSO4]	1-ethyl-3-methylimidazolium ethyl sulfate	1061.1	40.4	676.8	0.3368
[bmim][TfO]	1-butyl-3-methylimidazolium trifluoromethanesulfonate	1016.3	29.4	767.6	0.3677
[emim][TfO]	1-ethyl-3-methylimidazolium trifluoromethanesulfonate	985.2	35.8	653.4	0.2891
[bmim] [Ntf2]	1-butyl-3-methylimidazolium trifluoromethanesulfonate	1265.0	27.6	1007.1	0.2656
[hmim] [Ntf2]	1-hexyl-3-methylimidazolium trifluoromethanesulfonate	1287.3	23.9	1121.3	0.3539
[bmim] [Br]	1-butyl-3-methylimidazolium bromide	834.9	29.8	583.3	0.4891
[bmim] [dca]	1-butyl-3-methylimidazolium dicyanamid	1035.8	24.4	712.0	0.8419

[a] IUPAC is an acronym for International Union of Pure and Applied Chemistry.

the two constants of A and B for twenty ILs, respectively:

$$A = \log\ [P_c(T_c - 43)(T_c - T_b)] \tag{22}$$

$$B = \log\left[P_c(T_c-43)\frac{(T_b-43)}{(T_c-T_b)}\right] \tag{23}$$

The values for vapor pressure are accurate based on the generalized correlations and EOSs [66].

Knudsen strategy introduces another method to determine the vapor pressure of ILs. Knudson equation for calculation of ILs vapor pressure is as follows [67]:

$$P^{sat} = \left(1 + \frac{kS}{S'\alpha}\right)\frac{\Delta m}{kS\tau}\sqrt{\frac{2\pi RT}{M}} \tag{24}$$

where Δm stands for the mass loss during an elapsed time τ, S refers to the orifice area, k is the transmission coefficient, M signifies the molecular weight of a vapor, S' denotes the surface area of a liquid which is assumed to be equal to the cross-section area of a cell, and α represents the vaporization coefficient.

Vladimir et al. [68] measured the vapor pressure using the transpiration method and compared them with the values obtained from the Knudsen technique. They also introduced a relationship to calculate the saturation (vapor) pressure (P^{sat}) at different temperatures. The following equation is utilized to obtain the vapor pressure [78]:

$$R \ln P^{sat} = a + \frac{b}{T} + \Delta_l^g C_p \ln\left(\frac{T}{T_0}\right) \tag{25}$$

In Eq. (25), T_0 is the reference temperature (298.15 K) and $\Delta_l^g C_p$ represents the difference between the heat capacities of gas and liquid phases [68].

Thermogravimetric analysis (TGA) is also a promising method for rapid determination of vapor pressure. Eq. (26) proposed by Langmuir can be used to calculate the vapor pressure based on the evaporation rate [69]:

$$\frac{dm}{dt} = \alpha\sqrt{\frac{M}{3\pi RT}}P^{sat} \tag{26}$$

where dm/dt is the evaporation rate, α is the evaporation coefficient, M is the molecular weight of vapor, and T and P^{sat} denote the temperature and vapor pressure, respectively. α depends on experimental conditions. Phang et al. [70] suggested a reference substance similar to the experimental substance in terms of boiling and melting points and molecular structure so that α can be assumed constant. Thus, the vapor pressure of a substance S (as a sample) can be expressed by the following equation:

$$P_S^{sat} = \left(\frac{M_{ref}}{M_S}\right)^{0.5}\frac{\left(\frac{dm}{dt}\right)_S}{\left(\frac{dm}{dt}\right)_{ref}} \tag{27}$$

M_{ref} and M_s represent the molecular weight of the reference and sample, respectively. They concluded that the vapor pressures obtained through evaporation data are reliable where the TGA method is employed [71].

In general, physical and thermodynamic properties of ILs including heat capacity, viscosity, density, solubility, excess enthalpies, and vapor-liquid equilibrium data of the water/CO_2/ILs mixtures are necessary to evaluate ILs for CO_2 capture and to design the absorption processes [72].

5. Characterization of CO_2/IL systems

5.1. Experimental methods

It is vital to investigate the thermodynamic properties of the substances which are utilized in the CO_2 capture processes so that the appropriate equipment are chosen to attain the ultimate separation goal. There are several experimental methods developed by researchers and research centers to determine the thermodynamic properties of various ILs, CO_2, and their mixtures.

High pressure phase equilibria experiments are traditionally classified as analytical systems when the composition is identified. They are referred to the synthetic systems if only the overall composition is known. Sub-classifications are based on the mobility of the sample. In the dynamic systems, one or more phases are recirculated outside the equilibrium cell. However, in the static methods, the sample is agitated in a closed cell. The volume of the cell can be constant or variable. A summary of common techniques for obtaining thermodynamic phase equilibria parameters is depicted in Fig. 9.

The common methods to determine the CO_2 solubility in an IL without sampling are the gravimetric analysis, pressure drop method, and gas chromatography. Gravimetric analysis is an analytical method which describes the quantitative determination of gas solubility through measuring the overall weight variation of a sample over the absorption process [17]. The schematic of the basic components of a gravimetric system is demonstrated in Fig. 10(a). The pressure drop method is a synthetic technique. In this methodology, the system volume and temperature are held constant and the pressure difference is recorded during gas absorption [74]. A schematic of a pressure drop equipment is shown in Fig. 10(b). Since ILs have a negligible vapor pressure, the changes in pressure are assumed to be due to the gas absorption. Thus, the gas absorbed by the IL can be determined. Solubility data from a gas chromatography equipment can be achieved through employing a systematic procedure. The solvent (IL) is saturated with the solute (CO_2) and then coated on a column. A non-absorbing carrier gas is directed into the column to extract CO_2 from the IL. The carrier gas is then analyzed in the gas chromatograph. This procedure determines the amount of absorbed CO_2 [74]. The pressure drop and synthetic methods are simpler than the gravimetric analysis and their results have higher sensitivity; but, their precision is lower [74].

According to Blanchard, Gu, and Brennecke [75], a pycnometer with a known volume can be used to determine the density of each pure

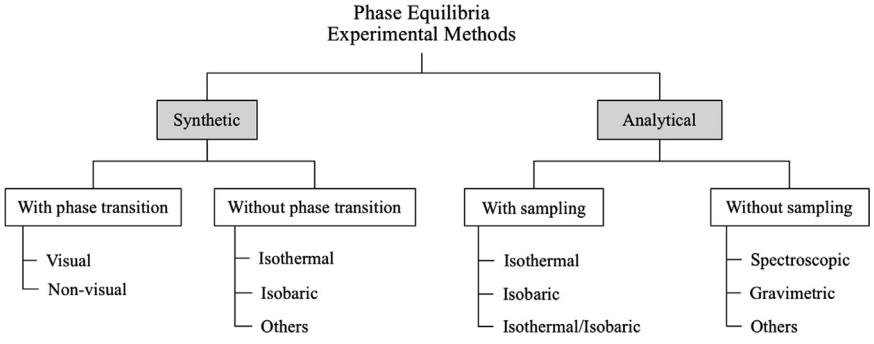

Fig. 9. Experimental methods to obtain phase equilibria data (modified after [73]).

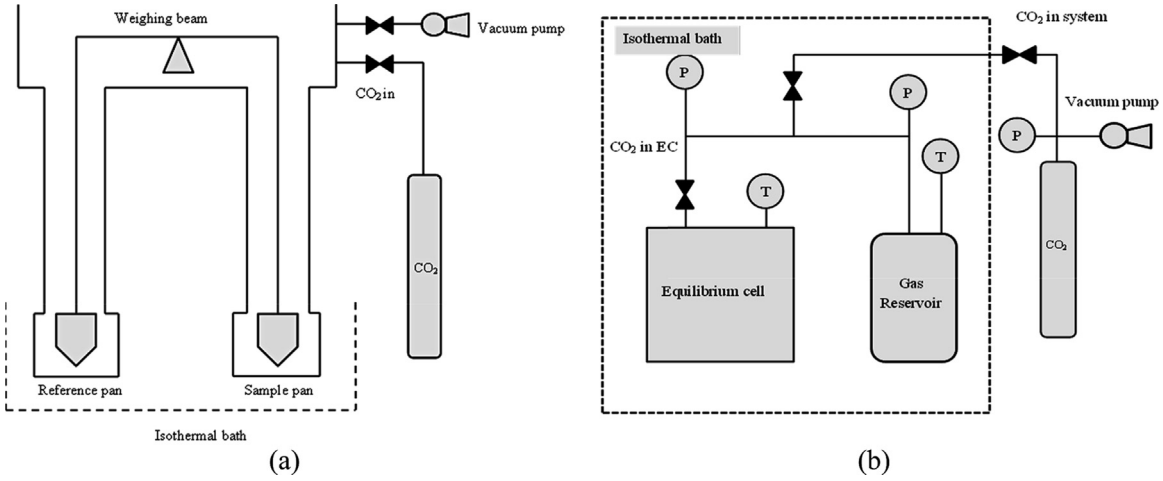

Fig. 10. : Schematics of: (a) a simple gravimetric system, including basic components, and (b) diagram for pressure drop method [P and T correspond to the pressure and temperature sensors, correspondingly] (modified after [17]).

Table 6
Summary of cubic EOSs widely used for VLE calculations [78].

EOS	Name	EOS or $P = P(V,T)$	Reference
vdW	van der Waals (1837)	$P = \frac{RT}{V-b} - \frac{a}{V^2}$	[78,79]
PR	Peng-Robinson (1976)	$P = \frac{RT}{V-b} - \frac{a}{V(V+b)+b(V-b)}$	[79]
PT	Patel-Teja (1982)	$P = \frac{RT}{V-b} - \frac{a(T)}{V(V+b)+c(V-b)}$	[80]
RK	Redlich-Kwong (1942)	$P = \frac{RT}{V-b} - \frac{a/T^{0.5}}{V(V+b)}$	[81]
SRK	Soave-Redlich-Kwong (1972)	$P = \frac{RT}{V+c-b} - \frac{a}{(V+c)(V+b+c)}$	[82]
PRSV	Peng–Robinson-Stryjek-Vera (1986)	$P = \frac{RT}{V-b} - \frac{a(T)}{(V+ub)(v+wb)}$	[83]

IL. The pycnometer is immersed in a constant-temperature bath and the amount of IL in the pycnometer is gravimetrically obtained where a thermal equilibrium is maintained [76]. The density of ILs can also be measured using a density measuring module such as DMA 4500 (manufacturer: Anton Paar GmbH). Another method for determination of IL density is with the aid of the proven oscillating U-tube principle that leads to a high accuracy [77].

5.2. Equations of state

It is important to study the vapor-liquid equilibrium (VLE) for the CO_2 capture processes to design and operate the separation stages [52]. One of the most common approaches to correlate and predict phase equilibrium is using equations of state (EOSs). According to Li [78], an EOS with a simple structure and reasonable accuracy is preferable, suggesting a cubic EOS is well suited to model phase equilibrium of multi-component systems. EOSs have been used to obtain the physical and thermodynamic characteristics of pure ILs and mixtures containing water, gases, and amines [61]. There are various EOSs; however, the most common EOSs are the cubic equations derived from van der Waals EOS. Among them, it has been proven that the Peng-Robinson (PR) EOS combines the simplicity and accuracy required for thermodynamic equilibrium calculations [52]. The well-known cubic EOSs are listed in Table 6. Li [78] reported that there are four cubic EOSs which are widely used in oil and gas industries, including: Peng-Robinson; Patel-Teja, Redlich-Kwong; and Soave-Redlich-Kwong.

The Peng-Robinson (PR) EOS can be used with different mixing rules to model the VLE of mixtures so that it can accurately predict important parameters such as gas and liquid volumes and vapor pressure [78]. In many chemical and petroleum engineering cases, the

Table 7
Parameters of EOSs [87].

EOS	General EOS parameters			
	δ	ε	θ	η
van der Waals (1890)	0	0	a	b
Redlich and Kwong (1949)	0	0	$a/(T_r^{0.5})$	b
Soave (1972)	b	0	$a\alpha(T)$	b
Peng and Robinson (1976)	$2b$	$-b^2$	$a\alpha(T)$	b
Patel and Teja (1982)	$b+c$	$-bc$	$a\alpha(T)$	b
Stryjek and Vera (1986)	$2b$	$-b^2$	$a\alpha(T)$	b

results obtained from EOSs are well matched with experimental data. Ren et al. [84] used the PR EOS with the van der Waals 2-parameter mixing rule to correlate VLE data for the CO_2-IL systems. A great agreement was attained between the experimental data and modeling outputs at all isotherms and pressures. However, Freitas et al. [117] claimed that the combination of the van der Waals 2-parameter mixing rule and the PR EOS does not lead to acceptable VLE results for some multi-component systems. Using a more complicated mixing rule such as the Wong-Sandler (WS) mixing rule was proposed for a number of multi-component mixtures. Based on Maia et al. [85], the PR EOS combined with the van der Waals and Wong-Sandler mixing rules is accurate at low pressures to model the VLE of binary systems; however, it does not offer reliable results at high pressures.

Another EOS, which is often addressed in the literature, is the Soave-Redlich-Kwong (SRK) EOS. According to Maia et al. [86], the PR EOS and SRK EOS are able to model the VLE data for most ternary systems with a total standard deviation of less than 0.03 and 0.04, respectively.

The general form of five-parameter EOSs is given below [87]:

$$P = \frac{RT}{V-b} + \frac{\theta\,(V-\eta)}{(V-b)\,(V^2+\delta V+\varepsilon)} \tag{28}$$

The parameters ε, θ, δ, and b might be constant or zero for a single component. They may depend on the composition of the mixture. These parameters are listed in Table 7.

In all EOSs listed in Tables 6 and 7, parameter b is a positive constant and equal to η. Parameters a and b are dependent on the critical properties of the component as expressed by the following equations:

$$a = a_c\,\alpha\,(T_r, \omega) \tag{29}$$

$$a_c = \frac{C_1 R T_c^2}{P_c} \tag{30}$$

Table 8
Temperature dependent parameter ($\alpha(T_r, \omega)$) for different EOSs [87].

Equation of state	$\alpha(T_r, \omega)$
van der Waals (1890)	1
Redlich and Kwong (1949)	$T_r^{-1/2}$
Soave (1972)	$[1 + (0.48 + 1.574\omega - 0.176\omega^2)(1 - T_r^{1/2})]^2$
Peng and Robinson (1976)	$[1 + (0.37646 + 1.5422\omega - 0.2699\omega^2)(1 - T_r^{1/2})]^2$
Patel and Teja (1982)	$(1 + [1 + (0.452413 + 1.38092\omega - 0.295937\omega^2)(1 - T_r^{1/2})]^2(1 - T_r^{1/2}))^2$
Stryjek and Vera (1986)	$[1 + (0.37889 + 1.48971\omega - 0.0.171318\omega^2 + 0.019655\omega^3)$ $(1 - T_r^{1/2})]^2 + k_1(1 - T_r)(0.7 - T_r)$

$$b = \frac{C_2 R\, T_c}{P_c} \tag{31}$$

where the parameter α is a function of temperature and acentric factor.

C_1 and C_2 are the constants, depending on the type of EOS. C_1 is 0.0778 for Peng-Robinson (PR) [79] and 0.0833 for Soave-Redlich-Kwong (SRK) [88]. C_2 is 0.4572 for PR and 0.4218 for SRK. $\alpha(T_r, \omega)$ is a temperature dependent parameter expressed in terms of the reduced temperature (T_r), as tabulated in Table 8.

Recently, some molecular-based models have been introduced which are more suitable for both complex and simple molecule structures. For instance, Chapman et al. [89] proposed the statistical associating fluid theory (SAFT), which uses a reference fluid that incorporates the chain length and molecular association. The reference fluid utilized in SAFT is simpler than the hard sphere reference fluid used in most of EOSs. This EOS provides useful thermodynamic basis through employing the chemical potential or fugacity concept to take into account the effects of molecular structure and interactions on the phase behavior and properties of fluids [6]. In late 1990, different versions of SAFT such as SAFT-VR (for potentials of variable attractive range),[90] Soft-SAFT (built from a reference Lennard-Jones fluid) [91,92], and PC-SAFT (perturbed-chain SAFT) [93] have been developed for improving the accuracy of the reference fluid term. According to the literature, the perturbed-chain statistical associating fluid theory (PC-SAFT) is a suitable model to simulate thermodynamic behaviors of pure ILs and binary systems of CO_2 and ILs.

The PC-SAFT equation is written in terms of Helmholtz free energy as the following:

$$\tilde{a}^{res} = \tilde{a}^{hc} + \tilde{a}^{disp} + \tilde{a}^{assoc} \tag{32}$$

in which, $\tilde{a}^{res}$ is the residual Helmholtz free energy of the system. The superscripts *hc*, *disp*, and *assoc* refer to a reference hard-chain contribution, a dispersion contribution, and an associating contribution, respectively. The following relationship also exists, according to PC-SAFT:

$$\tilde{a} = \frac{a}{RT} \tag{33}$$

The binary interaction parameters are normally used to match the modeling results with the experimental data. In some cases, if the van der Waals 2-parameter mixing rules are incorporated in EOSs, modeling of VLE through EOS is not feasible. Based on the previous studies, the Wong-Sandler mixing rules are a proper choice while studying CO_2-IL systems [94]. Further information on the mixing rules is found in Appendix.

5.3. Pressure-temperature-composition diagrams

To further understand the thermodynamic behaviors of CO_2/IL systems, it seems necessary to plot pressure-temperature -composition diagrams through experimental and modeling methods so that researchers/engineers can specify the thermodynamic state of mixtures at various process and thermodynamic conditions without conducting timely and difficult computational tasks.

In the literature, different models for obtaining VLE data with the aid of experimental data have been proposed. Generally, the differential evolution (DE) and differential evolution with Tabu List (DETL) show a better performance than simulated annealing (SA), genetic algorithm (GA), and particle swarm optimization (PSO) [95]. The DE approach is based on the difference between two individuals and adding it to another individual and generating a new individual.

The pressure-temperature (P-T) diagram is depicted in Fig. 11 for the CO_2/[omim][BF_4] system, based on the experimental data. The measured P-T data (isopleths) indicate the values at which the last tiny CO_2 bubble is completely dissolved in [omim][BF_4] at the equilibrium conditions [96]. A homogeneous liquid phase appears at higher pressures whereas at lower pressures, gas and liquid phases co-exist: a CO_2-rich phase and a [omim][BF_4]-rich phase [96]. Gutkowski et al. [97] found no critical points for any of the measured isopleths. It was concluded that the critical condition will not happen at temperatures below 363 K and pressures up to 100 MPa.

Fig. 12 shows a pressure-composition diagram for CO_2 in ten common imidazolium based ILs where the pressure is plotted against the CO_2 mole fraction at 298 K [98].

Another approach to attain appropriate and reliable properties of ILs and to experience high gas solubility of amines is using mixtures of ILs and amines. For example, Camper et al. [99] used two mixtures of alkanolamines, namely MEA and DEA with [Rmim][Tf_2N] ILs. Fig. 13 demonstrates CO_2 uptake by two mixtures of ILs-amine. They observed that the absorption performance of ILs-amine mixture is higher than pure amines and the desorption energy is lower. Furthermore, they do not exhibit the drawbacks of functionalized ILs.

Optimization algorithms are an important element for properly controlling processes and developing mathematical models with optimal variables [100]. Algorithms simplify calculations and can be used to help researchers determine the VLE data. This is vital as pressure-temperature -composition diagrams can provide important

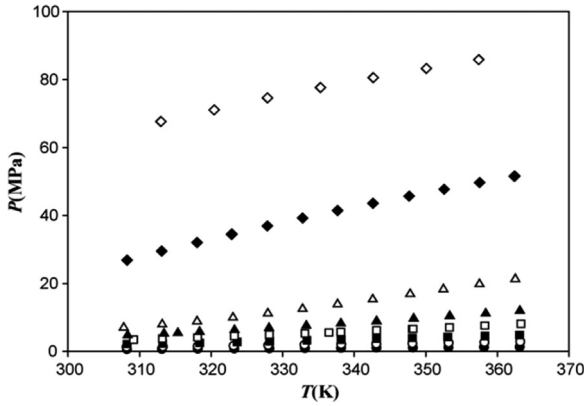

Fig. 11. P-T diagram for the CO_2/[omim][BF_4] system at different isopleths for x_{CO_2}: • 0.101, ○ 0.200, ■ 0.299, □ 0.412, ▲ 0.505, △ 0.602, ◆ 0.702, ◊ 0.752 [96].

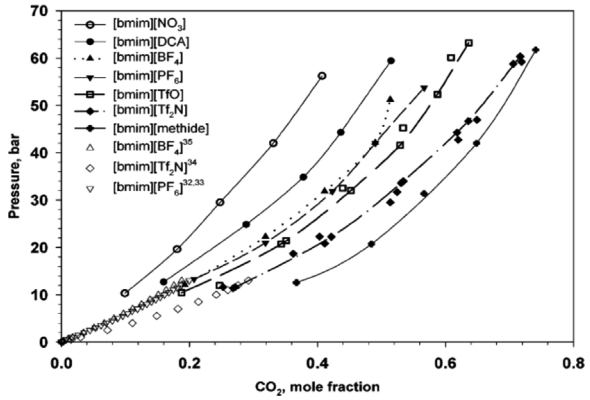

Fig. 12. Effect of the anion and pressure on the solubility of CO_2 in [bmim] cation based ILs at a temperature of 298 K [98].

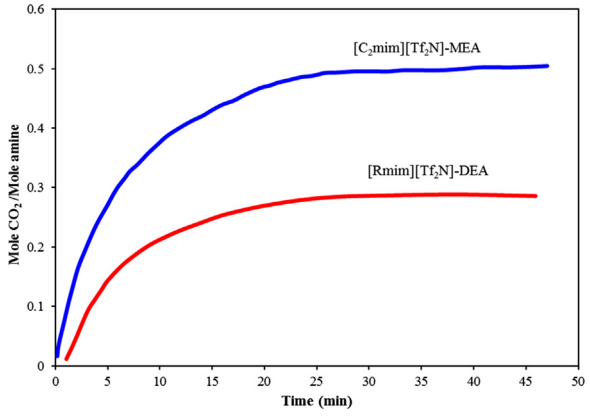

Fig. 13. CO_2 uptake in equimolar solutions of [C_2mim][Tf_2N]-MEA and [Rmim][Tf_2N]-DEA (modified after [99]).

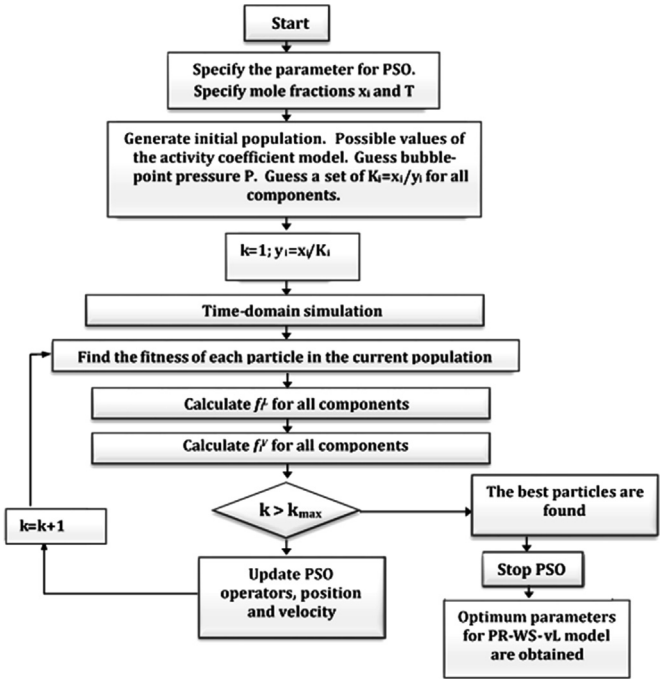
Start
Specify the parameter for PSO. Specify mole fractions xi and T
Generate initial population. Possible values of the activity coefficient model. Guess bubble-point pressure P. Guess a set of Ki=xi/yi for all components.
k=1; yi=xi/Ki
Time-domain simulation
Find the fitness of each particle in the current population
Calculate fi' for all components
Calculate fi'' for all components
k > kmax
The best particles are found
k=k+1
Update PSO operators, position and velocity
Stop PSO
Optimum parameters for PR-WS-vL model are obtained

Fig. 14. : PSO algorithm diagram for vapor-liquid equilibrium modeling [101].

Table 9
Average absolute deviations of experimental and calculated data for equilibrium (saturation) pressure [6,106].

Models	Ionic liquids	*AAD (%)*		
		303.15 K	313.15 K	Average
PR/WS/vL	[C_2-mim][Tf_2N]	4.50	4.10	4.30
	[C_4-mim][Tf_2N]	5.41	3.91	4.66
	[C_6-mim][Tf_2N]	5.80	4.81	5.31
	[C_8-mim][Tf_2N]	4.81	4.98	4.89
PR/vdW	[C_2-mim][Tf_2N]	12.10	13.50	12.75
	[C_4-mim][Tf_2N]	11.71	11.00	11.35
	[C_6-mim][Tf_2N]	9.70	9.61	9.65
	[C_8-mim][Tf_2N]	10.61	9.90	10.25
PC-SAFT	[C_2-mim][Tf_2N]	4.42	3.90	4.16
	[C_4-mim][Tf_2N]	4.93	6.92	5.93
	[C_6-mim][Tf_2N]	8.23	6.71	7.47
	[C_8-mim][Tf_2N]	8.06	9.17	8.61

thermodynamic data through a simple, straightforward, and understandable manner.

Particle swarm optimization (PSO) is an algorithm based on a social-psychological metaphor; a population of individuals (referred to particles) adapts by returning stochastically towards previously successful regions [101]. According to Lazzús [101], the PSO algorithm is appropriate to obtain the optimal values of important parameters involved in the VLE of binary systems containing supercritical fluids and ILs. Providing further information, the proposed PSO algorithm evaluates the binary interaction parameters with high accuracy. Lazzùs [101] compared the results obtained from the PSO and Levenberg-Marquart (LM) algorithms. It was found that the PSO algorithm estimates VLE information of the system more accurate than LM. The flow diagram of the PSO algorithm to determine VLE data is shown in Fig. 14.

Lazzus [102] also introduced a hybrid model including artificial neural network (ANN) and particle swarm optimization (PSO) for prediction of the thermodynamic properties.

5.4. Experimental and modeling data for thermodynamic properties

There are advantages and disadvantages with both experimental and modeling approaches to forecast the thermodynamic properties and behaviors of CO_2-IL systems. Experiments provide useful thermodynamic information. However, conducting experiments is costly and time consuming. The costs associated with the experiments also limit the amount of ILs to be used in the tests. On the other hand, the modeling data are associated with some inherent errors due to assumptions, convergence, and solution method drawbacks [103]. Tables 9–11 represent the experimental CO_2 solubility data for imidazolium, phosphonium, pyridinium, pyrrolidinium, and functionalized ILs. It is important to compare experimental and modeling data to ensure that the appropriate model is chosen for the process and the model is accurate enough to predict the system's behaviors. Table 9 shows the absolute average deviations, in percentage, between the experimental and modeling data of the PC-SAFT EOS and PR EOS where Wong-Sandler/van Laar (WS/vL) mixing rules and van der Waals (vdW) mixing rules are employed. These results show that the PR/WS/vL model predicts the high-pressure solubility of CO_2 in [C_n-mim][Tf_2N] more accurate than PR/vdW model under pressures up to the supercritical region of CO_2 [94]. PC-SAFT EOS was used to compare the experimental solubility data of CO_2 in the imidazolium based ILs. It was found that PC-SAFT EOS is able to estimate the solubility in a good agreement with experimental data [6]. PC-SAFT parameters can be determined using a correlation in terms of density and vapor pressure data of ILs. Hence, the parameters can be obtained without carrying out experiments. The binary interaction of ILs (as discussed before) is temperature dependent and increases linearly with temperature. The

Table 10
CO_2 solubility experimental data for imidazolium-based ionic liquids.

Ionic liquid	T (K)	P (bar)	Max solubility[a] (mol CO_2/mol IL)	H (bar)	Reference
[hmim][FEP]	283.15, 298.6, 323.2	0.297-18.1	0.517	18.5	[107]
[bmpyrr][FEP]			0.498	20.3	
[ETT][FEP]			0.497	20.8	
[bmim][PF_6]	293-393	1-97	0.555	12.0	[108]
[bmim][PF6]	283-348	0.096-19.99	0.379	34.0	[109]
[bmim][BF4]			0.364	38.0	
[bmim][PF_6]	313.15, 323.15, 333.15	0.97-92	0.729	N/A	[75]
[C_8mim][PF_6]			0.755		
[C_8mim][BF_4]			0.513		
[bmim][NO_3]			0.708		
[emim][$EtSO_4$]			0.579		
[N-bupy][BF_4]			0.423		
[C_2-mim][Tf_2N]	301-344.4	10-43	0.761	N/A	[110]
[C_4-mim][Tf_2N]			0.803		
[C_6-mim][Tf_2N]			0.833		
[C_8-mim][Tf_2N]			0.845		
[bmim] [DCA]	298.15, 313.15, 333.15	1-120	0.550	N/A	[98]
[bmim] [NO_3]			0.475		
[bmim] [BF_4]			0.520		
[bmim] [PF_6]			0.640		
[bmim] [TfO]			0.641		
[bmim] [Tf_2N]			0.681		
[bmim] [methide]			0.761		
[bmim][NO_3]			0.442		

[a] Maximum solubility in the range of tested operating conditions.

binary interaction can be obtained by curve-fitting of the experimental vapor- liquid equilibrium data, and a correlation can be determined using the group contribution method. As shown in Table 9, PC-SAFT EOS estimates the solubility of CO_2 in ILs with a higher accuracy, compared to cubic EOSs.

In recent years, advanced EOS have been developed in the framework of statistical mechanics and have been proven promising due to their capability to accurately simulate complicated systems [104,105]. Arguably, the most widely used EOSs in this context are the Statistical Associating Fluid Theory (SAFT) and the Perturbed Chain-SAFT (PC-SAFT) [104].

The SAFT and PC-SAFT EOSs were proposed to overcome the drawbacks of cubic EOSs, especially in estimating the density and compressibility factor of liquid phases. The cubic EOSs do not consider the effect of association and cross association of molecules on the phase equilibria. This will be an important feature in the IL-CO_2 systems. The PC-SAFT EOS incorporates the influence of molecular association on the volume and energy, and can potentially predict a more precise and reliable phase behavior when the association between the molecules becomes important. The SAFT parameters have the physical significance, featuring diameter, number of segments, and segment-segment interactions [105]. Therefore, the SAFT EOSs consider the effect of molecular structure and interactions on the bulk properties and phase behavior unlike the cubic EOSs that assume molecules as a hard sphere [6].

Based on the experimental and modeling investigations available in the open sources, the proper cubic EOSs to reasonably simulate the thermodynamic behaviors of CO_2-IL systems are also reported in this study (see Table 6) where modifications on the mixing rules and interaction terms of the cubic EOSs have been made to attain a good agreement between the real data and modeling outputs [78].

As Eq. (34) shows, AAD in Table 9 stands for the average absolute deviation which represents the difference between the experimental and calculated target parameter(s).

Table 11
CO_2 solubility for phosphonium, pyridinium, and pyrrolidinium ionic liquids.

Ionic liquid	T(K)	P(bar)	Max Solubility[a] (mol CO_2/mol IL)	H (bar)	References
[THTDP][NTf_2]	293.2–363.2	1.06–375	0.879	19.8	[111]
[THTDP][Cl]			0.800	18.9	
[N-bupy][BF_4]	313.15,323.15, 333.15	0.97–91.9	0.581		[75]
[$P_{(14)666}$][Cl]	303.15	1		36	[112]
[$P_{(14)666}$][DCA]			0.033	29	
[$P_{(14)666}$][Tf_2N]				37	
[$P_{(2)444}$][DEP]				59	
[$P_{(14)444}$][DBS]				29	
[$N_{(4)113}$][Tf_2N]				65	
[$N_{(6)113}$][Tf_2N]				53	
[$N_{(10)113}$][Tf_2N]				43	
[$N_{(4)111}$][Tf_2N]				61	
[$N_{(6)111}$][Tf_2N]				N/A	
[$N_{(10)111}$][Tf_2N]				44	
[$N_{(1)888}$][Tf_2N]			0.034	29	
[$N_{(6)222}$][Tf_2N]				60	
[hmpy][Tf_2N]	283	1–10	0.200	25.8	[113]

[a] Maximum solubility in the range of tested operating conditions.

$$AAD(\%) = \frac{100}{n_{pts}} \sum_{i=1}^{n_{pts}} \left| \frac{P_i^{sat,\exp} - P_i^{sat,cal}}{P_i^{sat,\exp}} \right| \quad (34)$$

in which, n_{pts} represents the number of data points; $P^{sat,exp}$ represents the experimental saturation pressure; and $P^{sat,cal}$ denotes the calculated saturation pressure.

Table 12 shows the CO_2 solubility for functionalized ionic liquids at two different temperatures and pressures. Providing further clarification on Table 12, functionality of NH_2 -Cation means that the group of NH_2 is attached to a chemical group in the IL to form the cation part of the functionalized IL. NH_2 -Anion refers to the combination of NH_2 group and a chemical branch in the IL structure to hold a negative charge, leading to formation of the anion part of the functionalized IL.

5.5. Effect of ions on thermodynamic behaviors

ILs are composed solely of anions and cations. It implies that there are many different combinations of ions that can be used to tailor ILs for various purposes. According to the literature, there are certain anions and cations that offer a higher performance for CO_2 capture processes. Brennecke and Maginn [116] found from their research study that the types of cations and anions significantly affect the chemical, physical, and thermodynamic properties of ILs. For instance, the anion part of ILs has the greatest effect on the solubility. According to Freitas et al. [117], the solubility is strongly related to the energy of vaporization and molar volume. As most of ILs have a high energy of vaporization, ILs with larger anions have higher molar volumes, leading to a greater CO_2 dissolution. It has been confirmed that the alkyl chain length of the cation has a major impact on the solubility of CO_2 in ILs. The alkyl group increases the dispersion forces of the cation for better interaction with CO_2, implying that growing the length of the alkyl chain leads to an increase in the CO_2 solubility [118].

The type of ions can also influence the melting point of the ILs. It was found that the melting point shows an ascending trend with increasing the chain length. When an IL contains a halide as an anion, the melting point is higher, compared to the cases having other anions [119].

The miscibility and hydrophobicity of ILs with water are also affected by the type of ions. For example, 1-alkyl-3-methylimidazolium hexafluorophosphate ILs are immiscible with water, while 1-alkyl-3-methylimidazolium nitrate ILs are completely miscible with water. Similarly, the hydrophobicity of an IL increases with increasing the chain length of the alkyl chain [120].

There is a correlation between the cation and the density where Uygur [87] concluded that the density of the IL lowers with increasing the alkyl chain length for the imidazolium cation case.

6. CO_2 solubility and selectivity

Flue-gas in practice contains various gases and impurities. Hence, the selectivity and solubility of CO_2 in ILs with respect to various gases such as N_2, CH_4, H_2, and H_2S should be evaluated. In this section, solubility of CO_2 in ILs and its selectivity in the presence of different gases will be discussed.

6.1. CO_2 solubility in ILs

It has been found that anions have a higher impact, compared to cations, on the solubility of CO_2 in ILs [121]. The CO_2 solubility in ten distinct imidazolium-based ILs was evaluated by Sudhir et al. [98]. They observed that the highest and lowest CO_2 solubility can be obtained in the ILs with fluoroalkyl groups in the anion part (e.g., [methide] and $[Tf2N]^-$) and nonfluorinated inorganic anions (e.g., $[NO3]^-$ and $[DCA]^-$), respectively. Their experiments also showed that the solubility strongly depends on the type of anions. However, in the smaller extent, the CO_2 solubility can be affected by the selection of alkyl groups on the cation part. In general, when the length of alkyl chain increases from butyl to octyl, the CO_2 solubility increases [98]. Molecular dynamic simulations show that the imidazolium-based ILs have better performance in terms of CO_2 capture than phosphonium-based ILs, where the same cation and anion are in the structure of ILs. For instance, $[Tf_2N]^-$ is more efficient, compared to $[PF6]^-$ [122]. Zhang et al. [107] used COSMO-RS and conducted a series of experiments to investigate the CO_2 capture by ILs. They determined the Henry's law constants of CO_2 with different combinations of the cations and anions. Their results implied that [FEP] anion has the greatest CO_2 solubility. Their experiments on three different cations with [FEP] anion revealed that CO_2 is more soluble in [hmim][FEP] (imidazolium based IL) than other ILs. Solubility and other properties including Henry's law constant, enthalpies, and entropies of nine gases dissolved in common imidazolium based IL ([bmim][PF6]) were studied where the pressure was up to 13 bar and three distinct temperatures (10, 25, and 50 °C) were examined. The experimental results showed that the highest and lowest solubilities in [bmim][PF6] are obtained for carbon dioxide and oxygen, respectively. It was also concluded that [bmim][PF6] (compared to common organic solvents) is not a very good solvent for reactions containing H_2, O_2, and CO (e.g., hydrogenation reactions, oxidation reactions, and hydroformylation reactions) for industrial purposes at extremely high pressures [18].

Solubility of CO_2 in ILs is an important factor to screen proper solvents and to design an efficient absorption system in CO_2 capture plants [123]. The solubility of gases in liquid solvents using Krichevsky-Kasarnovsky [124] equation is obtained as follows:

$$\ln \frac{f_2(T,P)}{x_2} = \ln H_2(P^{sat}) + \frac{V_2^{\infty}(P - P^{sat})}{RT} \quad (35)$$

where $f_2(T, P)$ represents the fugacity of gas solute in the gas phase at temperature T and pressure P; x_2 is the mole fraction of the gas dissolved in the liquid solvent; P^{sat} denotes the saturation or vapor pressure of the liquid solvents; V_2^{∞} refers to the partial molar volume of the

Table 12
CO_2 solubility for functionalized ionic liquids.

Ionic liquid	Functionality	P(bar)	T(K)	Max solubility (mol CO_2/mol IL)	H (bar)	References
$[P_{66614}][Ile]$	NH_2 -Anion	0–1.5	295.15	0.5	26	[114]
$[P_{66614}][Sar]$	NH_2 -Anion			0.523	1000	
$[P_{66614}][Gly]$	NH_2 -Anion			0.574	5.5	
$[P_{66614}][Pro]$	NH_2 -Anion			0.56	1000	
$[P_{66614}][Met]$	NH_2 -Anion			0.568	18	
APMim$[NTf_2]$	NH_2 -Cation	0–10	303	0.26		[115]
APMim[DCA]	NH_2 -Cation			0.29		
APMim$[BF_4]$	NH_2 -Cation			0.33		
AEMPyrr$[BF_4]$	NH_2 -Cation			0.27		
MeImNet2$[BF_4]$	NR_3- -Cation			0.25		
Bmim[Tau]	NH_2 -Anion			0.44		
Bmim[Gly]	NH_2 -Anion			0.4		

gas at the infinite dilution of the liquid solvents; H_2 stands for the Henry's law constant of the gas in the liquid solvents; R signifies the universal gas constant; and T is the temperature of the system. The Krichevsky-Kasarnovsky equation is often used to obtain the Henry's law constant from solubility data [124]. Thus, this equation is only limited to predicating the solubility of a gas in a liquid at low solubility conditions and should be avoided for the cases of CO_2 solubility in an IL with high magnitudes of solubility. It should be noted that the Henry's law is valid only if the concentration of a component in the liquid phase is minor.

The fugacity (f) of a pure gas can be determined using the following equation:

$$f(T, P) = \phi(T, P)P \quad (36)$$

in which, ϕ refers to the fugacity coefficient at pressure P and temperature T. This thermodynamic property can be obtained using various EOSs such as SRK and PR [36].

Maia et al. [86] claimed that all cubic-modified EOSs lead to almost the same accuracy while determining the solubility. In many cases, the Peng-Robinson (PR) and modified PR EOSs are appropriate EOSs to model the gas solubility. The PR EOS combined with the Wong-Sandler/UNIQUAC mixing rules can be used to estimate the Henry's law constant, which provides the gas solubility in a liquid solvent when the gas concentration in the liquid phase is small. This strategy helps to obtain the limiting slope defined by Henry's law as the solubility approaches zero [125]. According to Carvalho et al. [111], this methodology results in uncertainty that considerably affects the accuracy and reliability of the model outputs. Other models such as Predictive Peng-Robinson, Peng-Robinson-Stryjek-Vera, and Sanchez-Lacombe EOSs have been utilized to determine the gas solubility in ILs, exhibiting an error percentage less than 9.0% [37].

6.2. CO_2 selectivity

Due to the presence of gases and impurities in the flue-gas, the selectivity of CO_2 in ILs appears to be vital in carbon capture technique with ILs [126]. To systematically study the solubility of CO_2 in ILs, CO_2 selectivity in ILs needs to be investigated [127]. According to Zhang et al. [128], conventional ILs have a greater CO_2 selectivity, compared to other gases (e.g., CO, H_2, and O_2) due to the large quadrupole moment of CO_2. Since there is a mixture of different gases in the flue-gas, this high CO_2 selectivity is interesting, implying that ILs absorb CO_2 easier than other gases. In general, the solubility of CO_2 in ILs is higher than N_2 and H_2. However, the solubility of H_2 and N_2 exhibits an increase with increasing temperature [32,129]. In CO_2/H_2S systems, CO_2 selectivity is highly dependent on CO_2/H_2S feed ratio and CO_2 solubility is remarkably decreased in the presence of H_2S [35]. Ramdin et al. [130] showed that the selectivity of CO_2/CH_4 in different phosphonium and imidazolium-based ILs significantly decreases with increasing temperature.

It seems necessary to optimize CO_2 selectivity in ILs in terms of gas composition and operating conditions. The selectivity generally increases the number of stages required for CO_2 capture processes and consequently the operating and capital costs. For instance, in the case of CO_2/H_2S /CH_4 systems at high temperatures, an additional step is required to separate H_2S and CH_4 from CO_2 [127].

7. CO_2 capture using ILs: performance and modifications

As discussed in the introduction, carbon capture processes, in general, are divided into three main categories, including pre-combustion, post-combustion, and oxy-combustion. Among these methods, the post-combustion is appropriate for retrofit plants and the industrialized absorption methods mainly employ the post-combustion technology. The current solutions for absorption method are amine-based solvents, since they have a high CO_2 capacity. The practical applications of ILs for CO_2 capture depend on their effectiveness, compared to the amines. It is believed that ILs can be tailored to have a comparable CO_2 capacity without having the disadvantages associated with amine-based solvents.

Due to the volatility of amine-based solvents, the processes, which use this type of solvents, consume a high amount of energy during the solvent regeneration stage, which leads to an extra cost to the entire CO_2 capture process. This cost can be significantly lowered or even eliminated through using ILs as the non-volatile solvents. The amine-based solvents are not environmentally friendly due to their volatility nature. They are unstable in nature, resulting in producing dangerous toxic materials such as nitrosamines, nitramines, and amides. It should be noted that nitrosamines are of the most concern as they are carcinogenic and noxious to humans even at low concentrations [17]. ILs due to their negligibly low vapor pressure are considered non-volatile. It means that they do not vaporize and therefore do not contaminate the atmosphere. Therefore, solvent losses are negligible. Amines also participate in various parts of absorption processes and produce waste which can eventually corrode the equipment. However, ILs are not usually corrosive due to their high thermal and chemical stability. ILs are normally degraded at temperatures higher than 300 °C and only cause corrosion to equipment if there are impurities in the ILs [17].

Conventional ILs capture carbon through physical absorption mechanisms. Although adjusting cations/anions in the ILs can enhance the solubility of CO_2 in conventional ILs, their CO_2 capture capacity is still low in comparison with the current commercial carbon capture technologies such as amine-based solvents [29]. Indeed, there are strong chemical interactions between amine and CO_2 ($-\Delta H$ = 80–130 kJ/mol) in the amine-based solvents which make amines favorable for CO_2 molecules. However, in the case of conventional ILs/ CO_2 systems, there is a comparatively weak forces ($-\Delta H$ = ~ 15 kJ/mol) between ILs and CO_2 molecules [26]. Among alkanolamines as the most common solvents for the absorption purpose, mono ethanol amine (MEA) is more efficient than other amines. The order of absorption rate for amines is as

Table 13
Comparison of properties of ILs with common solvents used for CO_2 capture [128,132,133].

Variable		Chemicals for CO_2 Capture				
		Conventional ILs	Task-Specific ILs	MEA (30 %wt)	DEPG	PC
Absorption type		Physical	Chemical	Chemical	Physical	Physical
Viscosity (cP)		20-2000	50-2000	18.98	5.8	3.0
Vapor pressure (bar) at 25°C		1.33×10^{-9}	1.33×10^{-9}	8.5×10^{-4}	9.73×10^{-7}	1.13×10^{-4}
ΔH_{abs} (kJ/mol CO_2) at 1bar and 40°C		~10- 20	~40-50	~85	~14.3	~15.9
CO_2 solubility (mol/mol) at 1bar and 20-40 °C		> 2.51	1.6	50-85	3.63	3.41
Selectivity	CO_2/CH_4	8-35		n/a	15	26
	H_2S/CO_2	2-10		1-2	8.8	3.3
	CO_2/H_2	50-150		n/a	77	126
	CO_2/N_2	30-100		n/a	50	117
Cost		200 $/5 gr	400 $/5gr	370 $/1L	80 $/1L	117 $/1L

following: MEA > DEA > AMP > DIPA > MDEA[131]. Popular solvents for the physical absorption processes are DEPG (Selexol process), methanol (Rectisol process), NMP or *N*-methyl-2-pyrrolidone (Purisol process), Morphysorb process, and Propylene Carbonate (Flour process) [132]. General comparison between CO_2 capture processes through conventional ILs and the most common used commercial solvents are provided in Table 13 [128].

As provided in Table 13, pure conventional ILs are not a promising option for the CO_2 capture processes. To overcome this drawback, task-specific or functionalized ILs with the ability of chemisorption rather than physisorption have been developed. In this type of ILs, suitable moieties such as amines are introduced in the conventional ILs [134]. In this property-modification process, CO_2 -philic functional groups are attached to ILs which can significantly increase the CO_2 capture capacity of ILs [135]. Task-specific ILs in the broad classification are divided into three groups including; cation-functionalized ILs, anion functionalized ILs, and dual amino-functionalized ILs. The experimental results show that the reaction mechanisms between the amine functionalized IL and CO_2 are similar to the mechanisms between the organic amine and CO_2. Carbon capture capacity of task-specific ILs is also comparable to alkanolamines [4].

Complicated synthesis and purification steps, high viscosity which leads to slow CO_2 diffusion mass transfer, and high production cost are the main challenges to use functionalized ILs for CO_2 capture [136]. For instance, Camper et al. [99] concluded that the synthesis of amine-functionalized imidazolium-based ILs requires several steps, implying that the process is not economical compared to the absorption processes that utilize conventional solvents such as MEA. Therefore, in order to improve CO_2 capture capacity and to avoid these drawbacks, mixing ILs with other appropriate compounds such as water and amines are proposed. In this approach, solubility increases due to the viscosity reduction of the IL in the presence of water [128]. This mixture preserves the favorable properties of ILs for CO_2 capture and overcomes the inherent drawbacks of ILs including high viscosity and cost [137]. A mixture of alkanolamines such as MEA and an IL can also increase energy efficiency, absorption rate, and CO_2 absorption capacity [6]. There are some research studies in the literature, focusing on this challenging topic [99,138–140]. Common IL-amine mixtures are MEA + 1-butyl-3-methylimidazolium tetrafluoroborate ([bmim][BF_4]) + H_2O and MEA + 1-(2-hydroxyethyl)-3-methylimidazolium ([hemim][DCA]) + H_2O. Xu et al. [141] conducted several experiments and found that the viscosity of two ILs, known as 1-(2-hydroxyethyl)-3-methyl-imidazolium dicyanamide ([C_2OHmim][DCA]) and 1-butyl-3-methylimidazolium ([Bmim][DCA]), which are 50 mPa.s and 7 mPa.s at 313.15 K respectively, lowers to 3.54 mPa.s through mixing with amine (MEA). According to another study carried out by Yang et al. [139], the viscosity of an IL-amine solution including [bmim][BF_4] (as an IL) is 3.54 mPa.s at 323 K, which is much lower than the viscosity of the conventional [bmim][BF_4] (e.g., 31.08 mPa.s). The low viscosity of the IL-amine systems conveys the message that a higher mass transfer occurs where they are in contact with CO_2 such that more CO_2 is absorbed at a faster rate, which is favorable for the CO_2 capture operations.

It should be noted that when the conventional amines are used for

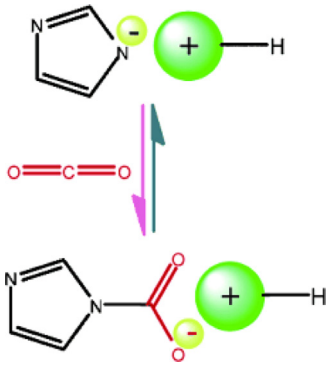

Fig. 15. CO_2 absorption mechanism of super basic ILs [144].

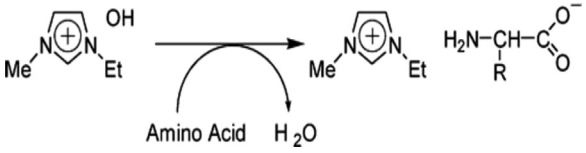

Fig. 16. General reaction leading to production of amino acid IL [143].

CO_2 capture, the energy consumption is fairly high which can be considerably decreased by utilizing an IL-amine system [99]. Based on the literature, when the content of ILs is 30 wt%, the energy consumption lowers by 27%, in contrast to the conventional MEA processes. However, if the concentration of ILs is lower than 10 wt%, the presence of ILs in aqueous 30 wt% MEA might decrease the required energy during the regeneration process without affecting the absorption efficiency/performance [141]. This increase in the energy efficiency would be beneficial as it would cause a decrease in the total costs of CO_2 capture processes. Table 14 summarizes various characters of three types of IL mixtures discussed in this section.

Recently, a new generation of the task specific ILs such as super base and amino acid ILs with an equimolar CO_2 absorption capacity has been introduced. In the super basic task-specific ILs, the CO_2 molecule from C atom is bonded to the nitrogen atoms in the anionic part of ILs, as shown in Fig. 15. Amino acids contain a carboxylic acid and an amino group which can be utilized as either an anion or a cation. Amino acid ILs have a promising carbon capture characteristic due to the presence of two functional groups, including carboxylic and amino groups. Furthermore, these ILs are more biodegradable, biocompatible, and easily producible in the large scales with low costs [142]. The general reaction of amino acid IL production is illustrated in Fig. 16 [143].

Recently, deep eutectic solvents (DESs) have been introduced as a new class of ILs. They have most of the promising properties of ILs and they are economically comparable to the amines for CO_2 capture. DESs are synthesized by ammonium and phosphonium salts with different hydrogen bond donors (HBDs) such as urea. Some DESs offer a higher CO_2 solubility and a lower viscosity, compared to ILs. Moreover, functionalized DESs promote a higher solubility for CO_2, compared to the conventional DESs [143,145,146]. It is important to note that CO_2

Table 14
Summary of advantages and disadvantages of three ionic liquid (IL) mixture systems [17].

Type	Advantages	Disadvantages
Conventional ILs (CILs)	• High CO_2 selectivity • Lower energy consumptions than conventional solvents	• High viscosity
Task-specific ILs	• Higher CO_2 storage capacity, compared to CILs (due to functional groups)	• Higher viscosities, compared to CILs • Complicated synthesis processes
IL-alkanolamine-water mixture	• Lower viscosities, compared to CILs • Higher CO_2 dissolution, compared to CILs	• Not environmentally friendly as pure ILs • Amine loss and energy consumption are lower for this type of ILs than amines but higher than CILs

Table 15
Prices for imidazolium, phosphonium, pyridinium, and guanidium-based ILs and tailored ILs [148].

IL-based	Cation	Anion	Price (CAD$)	Quantity (g)
Imidazolium	1-Allyl-3-methylimidazolium	bis(trifluoromethylsulfonyl)imide	160	5
		bromide	151	5
		chloride	113	5
		dicyanamide	150	5
		iodide	225	5
		chloride	90	5
	1-Benzyl-3-methylimidazolium	hexafluorophosphate	105	5
		tetrafluoroborate	125	5
		chloride	225	5
	1-Butyl-2,3-dimethylimidazolium	hexafluorophosphate	83	5
		tetrafluoroborate	99.4 (> 99%), 33(> 97%)	5
	4-(3-Butyl-1-imidazolio)	butanesulfonate	303	5
		acetate	331	5
		bis(trifluoromethylsulfonyl)imide	142	5
		bromide	71	5
		chloride	73	5
		dicyanamide	305	5
	1-Butyl-3-methylimidazolium	hexafluoroantimonate	105	5
		hexafluorophosphate	90(> 97%)	5
		hydrogen sulfate	149	5
		iodide	68	5
		tetrafluoroborate	45	5
	1,3-Dimethylimidazolium	dimethyl phosphate	46	5
		methyl sulfate	188	5
		tetrafluoroborate	43	5
		bis(pentafluoroethylsulfonyl)imide	339	5
		bis(trifluoromethylsulfonyl)imide	221	5
	1-Ethyl-2,3-dimethylimidazolium	chloride	40	5
		bromide	40	5
		dicyanamide	313	5
		tetrafluoroborate	275	5
		trifluoromethanesulfonate	103	5
		bis(trifluormethylsulfonyl)imide	185	5
	1-Hexyl-3-methylimidazolium	chloride	194	5
		hexafluorophosphate	87	5
	1-Methylimidazolium	chloride	135	5
Phosphonium	Tetrabutylphosphonium	Methanesulfonate	84	5
		Tetrafluoroborate	338	5
		p-toluenesulfonate	122	5
		bis(trifluoromethylsulfonyl)amide	56	5
		bis(2,4,4-trimethylpentyl)phosphinate	27	5
	Trihexyltetradecylphosphonium	Bromide	90	5
		Chloride	25	5
		Decanoate	90	5
		Dicyanamide	33	5
	Triphenylphosphonio	propane-1-sulfonate	258	5
	Triphenylphosphonio	propane-1-sulfonic	963	50
Pyridinium	1-Butyl-3-methylpyridinium	bis(trifluormethylsulfonyl)imide	175	1
		Hexafluorophosphate	156	5
	1-Butyl-4-methylpyridinium	Iodide	59	5
		Tetrafluoroborate	110	5
	1-Butylpyridinium	Bromide	97	5
	1-(3-Cyanopropyl)pyridinium	Chloride	158	5
	1-Ethylpyridinium	Tetrafluoroborate	90	5
	3-Methyl-1-propylpyridinium	bis(trifluormethylsulfonyl)imide	183	1
Guanidinium	Guanidinium	iodide	82.50	5
	Guanidinium	chloride	97	5
	Guanidine	thiocyanate	120	100
	Guanidine	thiocyanate (solution)	107.50	50 ml
Tailored	1-(3-Cyanopropyl)-3-methylimidazolium	bis(trifluoromethylsulfonyl)amide	439	5
	1-(3-Cyanopropyl)-3-methylimidazolium	chloride	390	5

solubility in amine-based DESs such as ChCl-DEA is much higher than conventional DESs and 30% (by weight) aqueous amines [145,146].

8. Economic analysis of CO_2 capture using ionic liquids

Currently, ILs are not as commercially available to the same extent as the amine-based solvents that are conventionally used in CO_2 capture. They are usually used at the lab scale which is very far from the industrial scale in terms of efficiency, operation, and cost. According to Arshad [147], there are several vendors such as Merck, Sigma Aldrich (Now MilliporeSigma), DuPont, Fluka, Scionix, Chemada, and Degussa that provide ILs for various purposes; however, most of ILs are produced at the laboratory scales and their prices are in the range of $1/g-$10/g. The cost should be reduced by a factor of approximately 100 or greater to be comparable with that of the conventional solvents. Ramdin et al. [26] reported that the lab-scale cost of ILs is around $1000/kg, which is 100–1000 times more expensive, compared to the conventional solvents. This price is expected to drop by $40/kg to $100/kg according to BASF company when ILs are produced at larger scales; however, it is still higher than the price of conventional solvents

by a factor of 10–20 due to the complexity and cost of the synthesis and purification stages. The prices of imidazolium based, phosphonium based, pyridinium based, and tailored ILs are listed in Table 15. As shown in Table 15, the conventional ILs are cheaper than the functionalized ones. In general, the tailored ILs are at least five times more expensive than most conventional ILs. It is worth mentioning that all prices are based on the official website of Sigma Aldrich (Now MilliporeSigma) company, accessed June 2017 [148].

Protic ILs with their simple acid-base chemistry are used in industrial processes and have a low cost (< $1.23/kg) which is comparable to that of the organic solvents such as toluene and acetone [149]. Also, the cost for synthesizing ILs with hydrogen sulfate (as the anion group) through acid-base neutralization is comparable with that of the organic solvents such as acetone and ethyl acetate ($1.34/kg to $1.4 /kg). For example, the prices of triethylammonium hydrogen sulfate and 1-methylimidazolium hydrogen sulfate are $1.24/kg, and $2.96/kg to $5.88/kg, respectively [150].

The total expenses of power plants include the costs for CO_2 capture from flue-gas (by amines) in the capital cost (CC) and operating costs (OC) [139]. Using ILs, some parts of the capital costs are less than those with amines. For example, in desorption process, ILs will be recovered completely due to low vapor pressure of the ILs. However, amines are volatile and some quantity of amines will be lost during the desorption process, leading to an increase in material and energy demands. Researchers found that using mixtures of ILs and amines, the energy consumption of the desorption stage lowers by more than 37%, compared to that with the amine solution [139].

Even though ILs are currently more expensive than the amines, their price is expected to be considerably decreased in the future. There are a large number of ILs available that can be synthesized through different ways. They have multiple-form markets such as their utilization as a solvent and catalyst with applications to reaction systems, separation systems, bio-refinery systems, energy storage, and GHG reducing media. These are great incentives for commercialization of functional ILs with low costs. Some of the benefits of ILs, compared to the amines, in CO_2 capture are as follows [17]:

- Less energy is required for regeneration of diluted ILs to remove the absorbed CO_2, than amines due to their physical absorption mechanisms.
- There is a low chance of being involved in a reaction with impurities and low probability of corrosion occurrence in the equipment due to the high thermal and chemical stability (> 300 °C) of ILs.
- There is no loss in the gas stream during regeneration due to the low vapor pressure of ILs.
- There are high potentials to produce a task-specific IL with manipulating anions and cations due to tunable nature of the ILs.

The separation cost consists of two parts including direct costs and indirect costs. The direct costs correspond to the costs of absorption and regeneration columns, lean/rich solvent heat exchangers, pumps, lean-solvent coolers, CO_2 compression unit, and other major equipment. The indirect costs include the general facilities, emergency, and owner's costs [151]. In addition, the operating and maintenance expenses (OME) should be considered. The OME consists of operating labor, maintenance costs, administrative and support labor costs, IL makeup, chemicals, solid waste treatment, power, and CO_2 transport and storage [151].

9. Screening of ionic liquids for CO_2 capture

Due to the tunability of ILs, room temperature ILs have 10^{18} possible structures [152]. This makes selection of the best ILs for CO_2 capture difficult. However, there are particular factors that should be considered to choose the most suitable ILs for CO_2 capture processes. These features include cost, ability of the IL to absorb CO_2, how well the IL will work at ideal conditions, and selectivity of CO_2 in the presence of various gases by the IL. There are also other factors such as the toxicity and biodegradability of the ILs if it is planned to use ILs in large quantities.

9.1. Economic prospect

As discussed before, ILs are currently expensive solvents. Their production processes are fairly difficult, which is a major obstacle while utilizing ILs for CO_2 capture at large scales. Many ILs are only available at the lab scales. Hence, it is not easy to estimate the total purchase cost if they are used in industrialized operations. The supplier Sigma-Aldrich is one of the ILs suppliers that provides the typical costs of a majority of ILs. It is clear that as the amount of the requested ILs increases, the price per gram drops significantly.

According to the prices listed for ILs by Sigma Aldrich (Now MilliporeSigma), the five best ILs in terms of economic aspect are: tributylmethylammonium chloride ([TBMA][Cl]); 1-butyl-3-methylimidazolium tetrafluoroborate ([bmim][BF4]); trihexyl(tetradecyl)phosphonium bromide ([P14666][Br]); trihexyl(tetradecyl)phosphonium chloride ([P14666][Cl]); and 1-ethyl-1-methylpyrrolidinium bromide ([C2Mpyrr][Br]). The prices of ILs at different scales are listed in Table 16.

9.2. Solubility and selectivity prospects

The CO_2 capture capacity of an IL is an important factor while choosing an IL for a CO_2 capture process. Researchers have studied many different ILs to determine what are the best in terms of their CO_2 solubility for the post-combustion CO_2 capture processes. It has been found that the anion of ILs has the greatest impact on the CO_2 capture capacity of ILs. According to the literature, the more fluorinated the anion is, the higher the CO_2 solubility is. It was also concluded that task-specific ionic liquids (TSILs) have a much greater CO_2 solubility than conventional ILs, since they are usually modified to absorb more CO_2.

Oliferenko et al. [153] provided a spreadsheet which lists many ILs and their corresponding Henry's law constants. Based on the data/information, the best ILs in terms of solubility are: 1-pentyl-3-methylimidazolium tris(nonafluorobutyl)trifluorophosphate ([$p_5$mim][bFAP]); trihexyl(tetradecyl)phosphonium chloride ([P_{14666}][Cl]); 1-hexyl-3-methylimidazolium tris(heptafluoropropyl)trifluorophosphate ([hmim][pFAP]); trihexyl(tetradecyl)phosphonium bis(trifluoromethylsulfonyl) imide ([P_{14666}][Tf_2N]); and methyltrioctylammonium bis(trifluoromethylsulfonyl)imide ([N_{1888}][Tf_2N]). The Henry's law constants for these ILs are presented in Table 17. It should be noted that the Henry's law constant represents the amount of CO_2 which is physically absorbed by an IL. In fact, it does not account for chemical absorption which can occur in TSILs.

The promising ILs in terms of selectivity of CO_2 and H_2S over other gases (e.g., methane) include BF_4, NO_3, and CH_3SO_4 anions and cations such as Tetrabutylammonium (N4111), Pentamethylguanidinium

Table 16
Prices for five potential ILs for CO_2 capture [148].

Ionic liquid	Weight (g)	Price (CAD$)	Price per weight (CAD$/g)
[TBMA][Cl]	100	129	1.29
	500	595	1.19
[bmim][BF4]	100	180.5	1.81
	1000	108.5	1.09
[P14666] [Br]	50	107.5	3.25
[P14666] [Cl]	5	35.5	7.10
	50	112.5	2.25
[C2Mpyrr] [Br]	5	36.2	7.24
	50	136	2.72

Table 17
Henry's law constant for potential ILs in terms of solubility [153].

Ionic Liquid	T (K)	Henry's law constant (bar)
[$p_5$mim][bFAP]	313	26.92
	303	22.44[a]
[hmim][pFAP]	313	28.84
	303	24.01[a]
[[P_{14666}][Cl]	303	23.99
[P_{14666}][Tf_2N]	303	26.30
[N_{1888}][Tf_2N]	303	38.18

[a] Linearly interpolated for comparison.

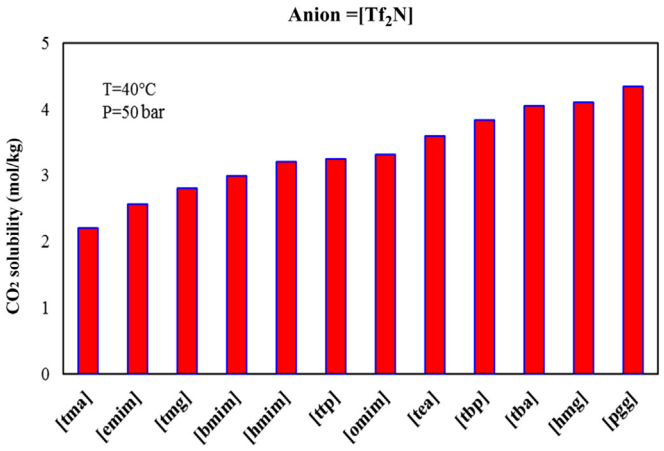

Fig. 17. Calculated CO_2 solubility in various ILs having an anion of Tf_2N [155].

(pmg), and Tetramethylguanidinium (tmg) [154].

Maiti [155] concluded that ILs containing pentamethylpropylguanidinium [ppg] cation and [BF4], [FEP], and [PF6] anions have a higher CO_2 solubility. The solubility data are illustrated in Fig. 17 and Fig. 18. Thus, the functionalized-guanidinium cations show a higher solubility than the imidazolium-based ILs [156,157]. Among anions, BF_4 and PF_6 are the best where the CO_2 solubility is the main selection criterion.

9.3. Operational condition prospects

Since high pressure and low temperature operations facilitate CO_2 absorption, the high pressure and low temperature conditions favor to absorb a high amount of CO_2. However, this is not appropriate for post-combustion processes, because increasing the pressure will increase the operating costs. Therefore, it is necessary to employ ILs that can attain an acceptable solubility of > 40% at the moderate temperature range of 293–313 K and the moderate pressure range of 5–10 bar. Several researchers have studied important absorption and characterization aspects of the amine-functionalized ILs, since they exhibit higher CO_2 absorption capacities due to chemical absorption, compared to conventional ILs. A part of functionalized ILs used for CO_2 capture are trihexyl(tetradecyl)phosphonium glycinate ([P_{14666}][Gly]), isoleucinate ([P_{14666}][Ile]), 2-cyanopyrrolide ([P_{14666}][2-CNpyr]), 3-(trifluoromethyl) ([P_{14666}][3-CF_3pyra]), prolinate ([P_{14666}][Pro]), and methionate ([P_{14666}][Met]) [26,114,135]. These studies reveal that non-conventional ILs are able to absorb CO_2 in a 1:1 stoichiometry at 295 K under low pressure conditions.

10. Main technical and practical challenges

Although thermodynamic models are very useful to characterize CO_2 and IL systems, there are still major challenges in this area. Adequate knowledge is required to select appropriate EOSs and mixing rules for complex systems such as H_2O/CO_2/IL. Inappropriate selection results in significant errors while predicting the thermodynamic characteristics [158,159].

The critical properties of CO_2 are available; however, finding the critical properties of the ILs is a challenging task, since they are decomposed at the normal boiling point. Hence, efficient methodologies need to be developed to accurately obtain the critical properties of ILs.

Thermodynamic models are often complex to be solved in phase equilibria for determination of the corresponding parameters. There are computational and software tools that may assist researchers. However, most of these approaches are expensive, difficult, and time-consuming. This poses another major challenge while employing thermodynamic models.

High viscosity of ILs, which leads to a decline in solubility of CO_2 in ILs, is one of the main challenges while utilizing ILs. There are some solutions for this challenge, which they need to be examined and investigated properly. One of the solutions is using mixture of water and amines with ILs, which the optimum composition and process conditions should be determined for these mixtures.

Another disadvantage of using ILs for CO_2 capture is the cost. ILs are more expensive, compared to amines. Although, the price of ILs in the large scale (less than $40/kg) can be much lower than currently available lab scale price (~ $1000/kg), the cost is still 10–20 higher

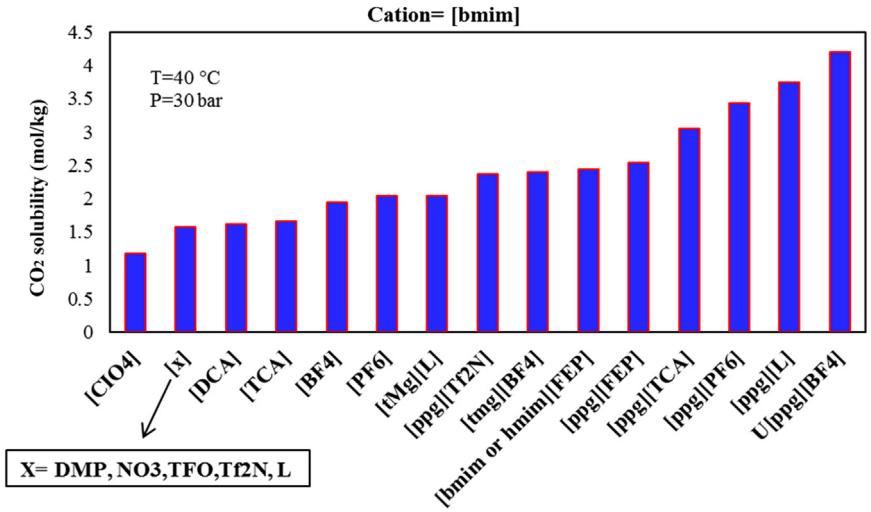

Fig. 18. CO_2 solubility in different ILs having a cation of bmim [155].

than the cost for conventional solvents [157]. Researchers need to find simple and economic synthesis solutions for CO_2 capture where the targeted solvent is an IL. To use ILs for absorption method in large scales, an appropriate system design and optimal operating conditions should be selected.

Recently, there have been new developments in CO_2 capture and utilization techniques such as introduction of efficient solid/liquid/gas systems with high CO_2 capture efficiency, utilization of a single liquid absorber to simultaneously capture CO_2 and SO_2, hydrogen production through employing chemical looping technique for CO_2 capture, electrofuels production from CO_2, and use of CO_2 for algae culturing [160–164]. However, more systematic engineering and research activities need to be conducted to assess the viability of the new strategies in terms of practical implication and economic and environmental prospects.

11. Conclusions

CO_2 capture processes involve several challenges in terms of technical, economical, and environmental prospects. Novel options for removal of CO_2 from flue-gases, including absorption with ionic liquids (ILs) have been proposed and investigated from thermodynamic, transport phenomena, and economic points of view. The CO_2 capture process using ILs is briefly explained in this review manuscript where the absorption mechanisms and the main practical and economic advantages and advantages are highlighted. The physical and chemical characteristics and the critical properties of CO_2 and ILs (and their mixtures) obtained from both experimental and modeling approaches are reported. The influences of important parameters such as type of anions and cations, ions length (size), IL volatility, and operating conditions on CO_2 solubility and selectivity are also discussed. Proper equations of state (EOSs) to study the vapor-liquid equilibrium of CO_2/ILs systems are reviewed in this paper. In addition, a comparison is made between the prices of the most common ILs that are considered as potential solvents in CO_2 capture processes. The cost of ILs plays an important role in their commercial utilization to absorb CO_2. The main conclusions are drawn as follows:

- Current CO_2 capture techniques generally suffer from high capital and operating costs, solvent degradation, high solvent losses, corrosive nature of solvents, toxicity of solvents, need of large absorption equipment, and high energy consumption in solvent regeneration.
- Among the EOSs, the results obtained by using PC-SAFT EOS showed great agreement with the experimental data at atmospheric and high pressures. Also, PR EOS results in good predictions where the Wong-Sandler/van Laar mixing rules are utilized.
- Although the functionalized or task-specific ILs are more suitable for the absorption of CO_2, they are 2–4 times more expensive than the conventional ILs.
- The best ILs in terms of technical and economic prospectives are screened. Based on this investigation, it is concluded that guanidinium cations and fluorine anions including [BF4], [FEP], and [PF6] are the best cation and anion, respectively as they exhibit a high CO_2 solubility.
- To commercialize CO_2 capture technology with ILs, it is vital to find cheap but suitable IL/additive mixtures with a relatively high solubility and selectivity where important mass transfer and thermodynamic prospects of CO_2/H_2O/IL/additive systems (diffusivity, mass transfer rate, vapor pressure, and equilibrium conditions) are well explored through experimental and modeling investigations.
- ILs, as green solvents, offer a promising CO_2 capture medium where an efficient absorption rate can be attained if a proper ion or chemical is added to IL. In addition to engineering design aspects of carbon capture processes, their high viscosity, cost, availability, compatibility, and purity are the main challenges to develop appropriate absorption systems to capture CO_2 using ILs at an industrial scale.

Acknowledgements

The authors would like to acknowledge the financial assistance of the Natural Sciences and Engineering Research Council of Canada (NSERC), InnovateNL, and Memorial University (MUN) in Canada.

Appendix. Mixing rules for equations of state

To use an EOS for mixtures, EOS constants should be obtained using mixing rules. Mixing rules include the binary interaction terms which represent the attractive and repulsive forces [158]. In general, the mixing rules are divided into two main categories including random and non-random mixing rules. The non-random mixing rules are used when the system contains asymmetric compounds such as water and methanol. The non-random mixing rules are represented by two terms; namely, conventional random mixing term and asymmetric term due to polarity.

The random mixing rules offer acceptable results in many practical cases. It is suggested that the mixing rules used in any EOS should attain the same form as that of the virial equation at conditions at which both equations are valid. The interactions between molecules in the multicomponent systems (the coefficients of virial equations) at low pressures are described as follows [159]:

$$a = \sum_i \sum_j x_i x_j (a_i .\ a_j)^{0.5}(1-k_{ij}) \tag{A.1}$$

$$b = \sum_i \sum_j x_i x_j b_{ij} = \sum_i \sum_j x_i x_j (b_i + b_j)/2 = \sum_i x_i b_i \tag{A.2}$$

$$a_{ij} = (a_i a_j)^{1/2}(1 - k_{ij}) \tag{A.3}$$

$$b_{ij} = [(b_i + b_j)/2](1 - k_{ij}) \tag{A.4}$$

$$b = \sum_i \sum_j x_i x_j (b_i + b_j)/2 \tag{A.5}$$

$$b = \frac{RT\sum_i \sum_j x_i x_j \left(b - \frac{a}{RT}\right)_{ij}}{RT - \left[\sum_i x_i \left(\frac{a_i}{a_j}\right) + \frac{G^E}{C}\right]} \tag{A.6}$$

Table A.1
Different mixing rules for EOSs [159].

Mixing rule	Equation
van der Waals	$a = \sum_i \sum_j x_i x_j (a_i.\ a_j)^{0.5}(1 - k_{ij})$
	$b = \sum_i \sum_j x_i x_j (b_i + b_j)/2$
Wong-Sandler	$a = b\left[\sum_i x_i \left(\frac{a_i}{a_j}\right) + \frac{G^E}{C}\right]$
	$b = \frac{RT \sum_i \sum_j x_i x_j \left(b - \frac{a}{RT}\right)_{ij}}{RT - \left[\sum_i x_i \left(\frac{a_i}{a_j}\right) + \frac{G^E}{C}\right]}$
Huron-Vidal	$a = b\left[\sum_i x_i \left(\frac{a_i}{a_j}\right) + \frac{G^E}{C}\right]$
Mathias-Klotz-Prausnitz	$a = \sum_{i=1}^{N} \sum_{j=1}^{N} x_i x_j \sqrt{a_i.\ a_j}(1 - k_{ij}) + \sum_{i=1}^{N} x_i \left(\sum_{j=1}^{N} x_j (\sqrt{a_i a_j I_{ji}})^{1/3}\right)^3$
	$b = \sum_i x_i b_i$

Once the parameters a and b are determined, they can be used in EOSs.

$$a = b\left[\sum_i x_i \left(\frac{a_i}{a_j}\right) + \frac{G^E}{C}\right] \tag{A.7}$$

$$a = \sum_{i=1}^{N} \sum_{j=1}^{N} x_i x_j \sqrt{a_i.\ a_j}(1 - k_{ij}) + \sum_{i=1}^{N} x_i \left(\sum_{j=1}^{N} x_j (\sqrt{a_i a_j I_{ji}})^{1/3}\right)^3 \tag{A.8}$$

$$b = \sum_i x_i b_i \tag{A.9}$$

$$\ln \frac{f_2(T, P)}{x_2} = \ln H_2 + \frac{V_2^{\infty}}{RT} P \tag{A.10}$$

$$f_2(T, P) = \phi(T, P) P \tag{A.11}$$

where b_{ij} represents the coefficients due to interaction between molecules i and j.

The attractive (a_{ij}) and repulsive (b_{ij}) forces between molecules i and j in the EOS can be expressed by the simple geometric and arithmetic average, respectively, through the following equations [159]:

$$a_{ij} = (a_i a_j)^{1/2} \tag{A.12}$$

$$b_{ij} = (b_i + b_j)/2 \tag{A.13}$$

Considering the attractive term between two non-similar molecules, the following binary interaction parameter (k_{ij}) should be added, as well [159]:

$$a_{ij} = (a_i a_j)^{1/2}(1 - k_{ij}) \tag{A.14}$$

For the repulsive term, if there is a high concentration of CO_2 in the system, another binary interaction parameter for the repulsion term (K'_{ij}) should be used as follows:

$$b_{ij} = [(b_i + b_j)/2](1 - K'_{ij}) \tag{A.15}$$

Common mixing rules that can be applied for ILs-CO_2 systems are given in Table A.1.

References

[1] Figueroa JD, et al. Advances in CO 2 capture technology—the US department of energy's carbon sequestration program. Int J Greenh Gas Control 2008;2(1):9–20.
[2] Bolin B, Eriksson E. Changes in the carbon dioxide content of the atmosphere and sea due to fossil fuel combustion. atmosphere sea Motion 1959;1:30–142.
[3] Coninck Hd. et al., IPCC special report on carbon dioxide capture and storage. Intergovernmental Panel on Climate Change; 2005.
[4] Yu KMK, et al. Recent advances in CO_2 capture and utilization. ChemSusChem 2008;1(11):893–9.
[5] Rahman FA, et al. Pollution to solution: capture and sequestration of carbon dioxide (CO_2) and its utilization as a renewable energy source for a sustainable future. Renew Sustain Energy Rev 2017;71:112–26.
[6] Chen Y, Mutelet F, Jaubert J-Nl. Modeling the solubility of carbon dioxide in imidazolium-based ionic liquids with the PC-SAFT equation of state. J Phys Chem B 2012;116(49):14375–88.
[7] Bailera M, et al. Power to Gas projects review: lab, pilot and demo plants for storing renewable energy and CO_2. Renew Sustain Energy Rev 2017;69:292–312.
[8] Sreedhar I, et al. Process and engineering trends in membrane based carbon capture. Renew Sustain Energy Rev 2017;68:659–84.
[9] (a) C.A.T. Force, Advanced post-combustion CO2 capture, 2009.
(b) Freund H, Bauer J, Zeiser T, Emig G. Detailed simulation of transport processes in fixed-beds. Ind Eng Chem Res 2009;44(16):6423–34
[10] Sreedhar I, et al. Carbon capture by absorption–path covered and ahead. Renew Sustain Energy Rev 2017;76:1080–107.
[11] Mirzaei S, Shamiri A, Aroua MK. A review of different solvents, mass transfer, and hydrodynamics for postcombustion CO_2 capture. Rev Chem Eng 2015;31(6):521–61.
[12] Global C, Institute (GCCSI)(2012) The Global Status of CCS: 2012. Canberra, Australia.
[13] Rochelle GT. Amine scrubbing for CO_2 capture. Science 2009;325(5948):1652–4.
[14] Riemer PW, Ormerod WG. International perspectives and the results of carbon dioxide capture disposal and utilisation studies. Energy Convers Manag 1995;36(6):813–8.
[15] Kothandaraman A. Carbon dioxide capture by chemical absorption: a solvent comparison study. Massachusetts Institute of Technology; 2010.
[16] Yu C-H, Huang C-H, Tan C-S. A review of CO_2 capture by absorption and

adsorption. Aerosol Air Qual Res 2012;12(5):745–69.
[17] Torralba-Calleja E, Skinner J, Gutiérrez-Tauste D. CO2 capture in ionic liquids: a review of solubilities and experimental methods. J Chem 2013;2013.
[18] Anthony JL, Maginn EJ, Brennecke JF. Solubilities and thermodynamic properties of gases in the ionic liquid 1-n-butyl-3-methylimidazolium hexafluorophosphate. J Phys Chem B 2002;106(29):7315–20.
[19] Johnson KE. What's an ionic liquid? Interface-Electrochem Soc 2007;16(1):38–41.
[20] Henni A, et al. Quantum-mechanical and thermodynamic study of amines and ionic liquids for CO_2 capture. Faculty of Graduate Studies and Research, University of Regina; 2013.
[21] Zhang S, et al. Physical properties of ionic liquids: database and evaluation. J Phys Chem Ref data 2006;35(4):1475–517.
[22] Wasserscheid P, Welton T. Ionic liquids in synthesis. 1. Wiley Online Library; 2008.
[23] Ghandi K. A review of ionic liquids, their limits and applications. Green Sustain Chem 2014;2014.
[24] Welton T. Room-temperature ionic liquids. Solvents for synthesis and catalysis. Chem Rev 1999;99(8):2071–84.
[25] Blanchard LA, et al. Green processing using ionic liquids and CO_2. Nature 1999;399(6731):28–9.
[26] Ramdin M, de Loos TW, Vlugt TJ. State-of-the-art of CO_2 capture with ionic liquids. Ind Eng Chem Res 2012;51(24):8149–77.
[27] Kirchner B. Ionic liquids. 290. Springer; 2009.
[28] Krupiczka R, Rotkegel A, Ziobrowski Z. Comparative study of CO 2 absorption in packed column using imidazolium based ionic liquids and MEA solution. Sep Purif Technol 2015;149:228–36.
[29] Shannon MS, Bara JE. Properties of alkylimidazoles as solvents for CO_2 capture and comparisons to imidazolium-based ionic liquids. Ind Eng Chem Res 2011;50(14):8665–77.
[30] Kroon MC, et al. Modeling of the carbon dioxide solubility in imidazolium-based ionic liquids with the tPC-PSAFT equation of state. J Phys Chem B 2006;110(18):9262–9.
[31] Yokozeki A, Shiflett MB. Gas solubilities in ionic liquids using a generic van der Waals equation of state. J Supercrit Fluids 2010;55(2):846–51.
[32] Shiflett MB, Yokozeki A. Separation of carbon dioxide and sulfur dioxide using room-temperature ionic liquid [bmim][MeSO4]. Energy Fuels 2009;24(2):1001–8.
[33] Andreu JS, Vega LF. Modeling the solubility behavior of CO_2, H2, and Xe in [C n-mim][Tf2N] ionic liquids. J Phys Chem B 2008;112(48):15398–406.
[34] Yokozeki A, et al. Physical and chemical absorptions of carbon dioxide in room-temperature ionic liquids. J Phys Chem B 2008;112(51):16654–63.
[35] Shiflett MB, Yokozeki A. Separation of CO2 and H2S using room-temperature ionic liquid [bmim][PF6]. Fluid Phase Equilibria 2010;294(1):105–13.
[36] Zhou L, Fan J, Shang X. CO_2 Capture and separation properties in the ionic liquid 1-n-Butyl-3-methylimidazolium nonafluorobutylsulfonate. Materials 2014;7:3867–80.
[37] Valderrama JO, Urbina F, Faúndez CA. Gas-liquid equilibrium modeling of mixtures containing supercritical carbon dioxide and an ionic liquid. J Supercrit Fluids 2012;64:32–8.
[38] Karakatsani EK, et al. tPC-PSAFT modeling of gas solubility in imidazolium-based ionic liquids. J Phys Chem C 2007;111(43):15487–92.
[39] Statistics I. CO2 emissions from fuel combustion-highlights. IEA, Pari; 2011. 〈http://www.iea.org/co2highlights/co2highlights.pdf〉. CitedJuly.
[40] Statistics IEAI. CO2 emissions from fuel combustion-highlights.: Paris; 2016.
[41] EIA U. International energy statistics [available at]. Washington, DC: US Energy and Information Administration; 2011 [available at]. 〈http://www.eia.gov/countries/data.cfm〉.
[42] Statistics O. Greenhouse gas emissions; 2017.
[43] 2016 on Track for Record Rate of Atmospheric CO2 Increase. 2016; Available from: 〈https://robertscribbler.com/2016/11/01/〉.
[44] Kurihara H, Shirayama Y. Effects of increased atmospheric CO_2 on sea urchin early development. Mar Ecol Progress Ser 2004;274:161–9.
[45] Matin A, et al. Canada's greenhouse gas inventory 1990–2002. Canada: Greenhouse Gas Division, Environment Canada Ottawa; 2004.
[46] Yalkowski S, He Y, Jain P. Handbook of aqueous solubility data second edition. New York: CRC Press; 2010.
[47] Haynes WM. CRC handbook of chemistry and physics. CRC press; 2014.
[48] Sovova H, Prochazka J. Calculations of compressed carbon dioxide viscosities. Ind Eng Chem Res 1993;32(12):3162–9.
[49] Fenghour A, Wakeham WA, Vesovic V. The viscosity of carbon dioxide. J Phys Chem Ref Data 1998;27(1):31–44.
[50] Austgen DM, et al. Model of vapor-liquid equilibria for aqueous acid gas-alkanolamine systems using the electrolyte-NRTL equation. Ind Eng Chem Res 1989;28(7):1060–73.
[51] Wilcox J. Carbon capture. Springer Science & Business Media; 2012.
[52] Palma Chilla L, Lazzús J, Pérez Ponce A. Particle swarm modeling of vapor-liquid equilibrium data of binary systems containing CO 2+ imidazolium ionic liquids based on bis [(trifluoromethyl) sulfonyl] imide anion. J Eng Thermophys 2011;20(4):487–500.
[53] Hayes R, Warr GG, Atkin R. Structure and nanostructure in ionic liquids. Chem Rev 2015;115(13):6357–426.
[54] Tomé LI, et al. Measurements and correlation of high-pressure densities of imidazolium-based ionic liquids. J Chem Eng Data 2008;53(8):1914–21.
[55] Dymond J, Malhotra R. The Tait equation: 100 years on. Int J Thermophys 1988;9(6):941–51.
[56] Bonhote P, et al. Hydrophobic, highly conductive ambient-temperature molten salts. Inorg Chem 1996;35(5):1168–78.
[57] Huddleston JG, et al. Characterization and comparison of hydrophilic and hydrophobic room temperature ionic liquids incorporating the imidazolium cation. Green Chem 2001;3(4):156–64.
[58] Valderrama J, Robles P. Critical properties, normal boiling temperatures, and acentric factors of fifty ionic liquids. Ind Eng Chem Res 2007;46(4):1338–44.
[59] Lydersen AL, Station MEE. Estimation of critical properties of organic compounds by the method of group contributions. University of Wisconsin; 1955.
[60] Joback KG, Reid RC. Estimation of pure-component properties from group-contributions. Chem Eng Commun 1987;57(1–6):233–43.
[61] Maia FM, et al. Modeling of ionic liquid systems: phase equilibria and physical properties. INTECH Open Access Publisher; 2013.
[62] Valderrama JO, Sanga WW, Lazzús JA. Critical properties, normal boiling temperature, and acentric factor of another 200 ionic liquids. Ind Eng Chem Res 2008;47(4):1318–30.
[63] Alvarez V, Valderrama J. A modified Lydersen-Joback-Reid method to estimate the critical properties of biomolecules. Alimentaria 2004;254:55–66.
[64] Valderrama JO, Rojas RE. Critical properties of ionic liquids. revisited. Ind Eng Chem Res 2009;48(14):6890–900.
[65] Valderrama JO, Forero LA. An analytical expression for the vapor pressure of ionic liquids based on an equation of state. Fluid Phase Equilibria 2012;317:77–83.
[66] Valderrama JO, Sanga WW. Critical properties and vapor pressure of twenty imidazolium based ionic liquids used in extraction bioprocesses. Frankfurt: Dechema Veranstaltungen; 2008.
[67] Paulechka Y, et al. Vapor pressure and thermal stability of ionic liquid 1-butyl-3-methylimidazolium Bis (trifluoromethylsulfonyl) amide. Thermochim Acta 2005;439(1):158–60.
[68] Emel'yanenko VN, Verevkin SP, Heintz A. The gaseous enthalpy of formation of the ionic liquid 1-butyl-3-methylimidazolium dicyanamide from combustion calorimetry, vapor pressure measurements, and ab initio calculations. J Am Chem Soc 2007;129(13):3930–7.
[69] Langmuir I. The vapor pressure of metallic tungsten. Phys Rev 1913;2(5):329.
[70] Phang P, Dollimore D, Evans SJ. A comparative method for developing vapor pressure curves based on evaporation data obtained from a simultaneous TG–DTA unit. Thermochim Acta 2002;392:119–25.
[71] Aschenbrenner O, et al. Measurement of vapour pressures of ionic liquids and other low vapour pressure solvents. Green Chem 2009;11(8):1217–21.
[72] Ficke LE, Novak RR, Brennecke JF. Thermodynamic and thermophysical properties of ionic liquid+ water systems. J Chem Eng Data 2010;55(11):4946–50.
[73] Dohrn R, Fonseca JM, Peper S. Experimental methods for phase equilibria at high pressures. Annu Rev Chem Biomol Eng 2012;3:343–67.
[74] Torralba-Calleja E, Skinner J, Gutiérrez-Tauste D. CO_2 Capture in ionic liquids: a review of solubilities and experimental methods. J Chem 2013:1–16.
[75] Blanchard LA, Gu Z, Brennecke JF. High-pressure phase behavior of ionic liquid/CO_2 systems. J Phys Chem B 2001;105(12):2437–44.
[76] Blanchard LA, Gu Z, Brennecke JF. High-Pressure Phase Behavior of Ionic Liquid/CO_2 Systems. J Phys Chem 2001;105:2437–44.
[77] Density Measuring Module: DMA 4500 ME, in Anton Paar.; 2016.
[78] Li H. Thermodynamic properties of CO2 mixtures and their applications in advanced power cycles with CO2 capture processes.; 2008.
[79] Peng D-Y, Robinson DB. A new two-constant equation of state. Ind Eng Chem Fundam 1976;15(1):59–64.
[80] Patel NC, Teja AS. A new cubic equation of state for fluids and fluid mixtures. Chem Eng Sci 1982;37(3):463–73.
[81] Redlich O, Kwong JN. On the thermodynamics of solutions. V. An equation of state. fugacities of gaseous solutions. Chem Rev 1949;44(1):233–44.
[82] Soave G. Equilibrium constants from a modified Redlich-Kwong equation of state. Chem Eng Sci 1972;27(6):1197–203.
[83] Stryjek R, Vera J. PRSV2: a cubic equation of state for accurate vapor—liquid equilibria calculations. Can J Chem Eng 1986;64(5):820–6.
[84] Ren W, Sensenich B, Scurto AM. High-pressure phase equilibria of {carbon dioxide (CO 2)+ n-alkyl-imidazolium bis (trifluoromethylsulfonyl) amide} ionic liquids. J Chem Thermodyn 2010;42(3):305–11.
[85] Maia FM, et al. Modeling of ionic liquid systems: phase equilibria and physical properties, in Ionic Liquids-New Aspects for the Future. InTech; 2013.
[86] Maia FM, et al. Equation of state modelling of systems with ionic liquids: literature review and application with the Cubic Plus Association (CPA) model. Fluid Phase Equilibria 2012;332:128–43.
[87] Uygur TJ. Experimental and thermodynamic studies of ionic liquids for carbon dioxide separation. Faculty of Graduate Studies and Research, University of Regina; 2013.
[88] Soave G. Improvement of the van der Waals equation of state. Chem Eng Sci 1984;39(2):357–69.
[89] Chapman WG, Jackson G, Gubbins KE. Phase equilibria of associating fluids: chain molecules with multiple bonding sites. Mol Phys 1988;65(5):1057–79.
[90] Gil-Villegas A, et al. Statistical associating fluid theory for chain molecules with attractive potentials of variable range. J Chem Phys 1997;106(10):4168–86.
[91] Pàmies JC, Vega LF. Vapor− liquid equilibria and critical behavior of heavy n-alkanes using transferable parameters from the soft-SAFT equation of state. Ind Eng Chem Res 2001;40(11):2532–43.
[92] Felipe J. Thermodynamic behaviour of homonuclear and heteronuclear Lennard-Jones chains with association sites from simulation and theory. Mol Phys 1997;92(1):135–50.
[93] Gross J, Sadowski G. Perturbed-chain SAFT: an equation of state based on a perturbation theory for chain molecules. Ind Eng Chem Res 2001;40(4):1244–60.
[94] Yazdizadeh M, Rahmani F, Forghani AA. Thermodynamic modeling of CO_2 solubility in ionic liquid ([Cn-mim][Tf2N]; n = 2, 4, 6, 8) using Wong-Sandler mixing

rule, Peng-Robinson equation of state (EOS) and differential evolution (DE) method. Korean J Chem Eng 2011;1:246–51.
[95] Zhang H, et al. Novel bare-bones particle swarm optimization and its performance for modeling vapor–liquid equilibrium data. Fluid Phase Equilibria 2011;301(1):33–45.
[96] Gutkowski KI, Shariati A, Peters CJ. High-pressure phase behavior of the binary ionic liquid system 1-octyl-3-methylimidazolium tetrafluoroborate + carbon dioxide. J Supercrit Fluids 2006;39:187–91.
[97] Gutkowski K, Shariati A, Peters C. High-pressure phase behavior of the binary ionic liquid system 1-octyl-3-methylimidazolium tetrafluoroborate+ carbon dioxide. J Supercrit Fluids 2006;39(2):187–91.
[98] Aki SN, et al. High-pressure phase behavior of carbon dioxide with imidazolium-based ionic liquids. J Phys Chem B 2004;108(52):20355–65.
[99] Camper D, et al. Room-temperature ionic liquid− amine solutions: tunable solvents for efficient and reversible capture of CO_2. Ind Eng Chem Res 2008;47(21):8496–8.
[100] Lazzús JA. Thermodynamic modeling based on particle swarm optimization to predict phase equilibrium of binary systems containing ionic liquids. J Mol Liq 2013;186:44–51.
[101] Lazzús JA. Optimization of high-pressure vapor-liquid equilibrium modelling of binary mixtures (supercritical fluid + ionic liquid) by particle swarm algorithm. Commun Math Comput Chem 2015;73:663–88.
[102] Lazzús JA. Neural network-particle swarm modeling to predict thermal properties. Math Comput Model 2013;57(9):2408–18.
[103] Klamt A, Eckert F, Arlt W. COSMO-RS: an alternative to simulation for calculating thermodynamic properties of liquid mixtures. Annu Rev Chem Biomol Eng 2010;1:101–22.
[104] Diamantonis NI, et al. Evaluation of cubic, SAFT, and PC-SAFT equations of state for the vapor–liquid equilibrium modeling of CO_2 mixtures with other gases. Ind Eng Chem Res 2013;52(10):3933–42.
[105] Ting PD, et al. Application of the PC-SAFT equation of state to asphaltene phase behavior, in Asphaltenes, heavy oils, and petroleomics. Springer; 2007. p. 301–27.
[106] Yazdizadeh M, Rahmani F, Forghani AA. Thermodynamic modeling of CO_2 solubility in ionic liquid ([C n-mim][Tf2N]; n = 2, 4, 6, 8) with using Wong-Sandler mixing rule, Peng-Rabinson equation of state (EOS) and differential evolution (DE) method. Korean J Chem Eng 2011;28(1):246–51.
[107] Zhang X, Liu Z, Wang W. Screening of ionic liquids to capture CO_2 by COSMO-RS and experiments. AIChE J 2008;54(10):2717–28.
[108] Perez-Salado Kamps A, et al. Solubility of CO_2 in the ionic liquid [bmim][PF6]. J Chem Eng Data 2003;48(3):746–9.
[109] Shiflett MB, Yokozeki A. Solubilities and diffusivities of carbon dioxide in ionic liquids:[bmim][PF6] and [bmim][BF4]. Ind Eng Chem Res 2005;44(12):4453–64.
[110] Shin E-K, Lee B-C, Lim JS. High-pressure solubilities of carbon dioxide in ionic liquids: 1-alkyl-3-methylimidazolium bis (trifluoromethylsulfonyl) imide. J Supercrit Fluids 2008;45(3):282–92.
[111] Carvalho PJ, et al. High carbon dioxide solubilities in trihexyltetradecylphosphonium-based ionic liquids. J Supercrit Fluids 2010;52(3):258–65.
[112] Kilaru PK, Scovazzo P. Correlations of low-pressure carbon dioxide and hydrocarbon solubilities in imidazolium-, phosphonium-, and ammonium-based room-temperature ionic liquids. Part 2. Using activation energy of viscosity. Ind Eng Chem Res 2008;47(3):910–9.
[113] Anderson JL, Dixon JK, Brennecke JF. Solubility of CO_2, CH4, C2H6, C2H4, O2, and N2 in 1-Hexyl-3-methylpyridinium Bis (trifluoromethylsulfonyl) imide: comparison to other ionic liquids. Acc Chem Res 2007;40(11):1208–16.
[114] Goodrich BF, et al. Experimental measurements of amine-functionalized anion-tethered ionic liquids with carbon dioxide. Ind Eng Chem Res 2010;50(1):111–8.
[115] Galan-Sanchez LM. Functionalised ionic liquids, absorptionsolvents for CO2 and olefin separation Ph.D. Thesis; 2008.
[116] Brennecke JF, Maginn EJ. Ionic liquids: innovative fluids for chemical processing. AIChE J 2001;47(11):2384–9.
[117] Freitas A, et al. Modeling vapor liquid equilibrium of ionic liquids+ gas binary systems at high pressure with cubic equations of state. Braz J Chem Eng 2013;30(1):63–73.
[118] Ren W, Sensenich B, Scurto AM. High-pressure phase equilibria of {carbon dioxide (CO_2) + n-alkyl-imidazolium bis(trifluoromethylsulfonyl)amide} ionic liquids. J Chem Thermodyn 2010;42:305–11.
[119] Brennecke JF, Maginn EJ. Ionic liquids: innovative fluids for chemical processing. Am Inst Chem Eng 2001;47(11):2384–9.
[120] Shariati A, Gutkowski K, Peters CJ. Comparison of the phase behavior of some selected binary systems with ionic liquids. Am Inst Chem Eng 2005;51(5):1532–40.
[121] Cadena C, et al. Why is CO_2 so soluble in imidazolium-based ionic liquids? J Am Chem Soc 2004;126(16):5300–8.
[122] YUE Z-g. et al., Molecular simulation on microstructure of ionic liquids in capture of CO2. 过程工程学报. **11**(4); 2011.
[123] Palma Chilla LO, Lazzús JA, Pérez Ponce AA. Particle swarm modeling of vapor-liquid equilibrium data of binary systems containing CO_2 + imidazolium ionic liquids based on Bis[(trifluoromethyl)sulfonyl]imide anion. J Eng Thermophys 2011;20(4):487–500.
[124] Carroll JJ, Mather AE. The system carbon dioxide-water and the Krichevsky-Kasarnovsky equation. J Solut Chem 1992;21(7):607–21.
[125] Carvalho PJ, et al. High carbon dioxide solubilities in trihexyltetradecylphosphonium-based ionic liquids. J Supercrit Fluids 2010;52:258–65.
[126] Xu G, et al. An improved CO_2 separation and purification system based on cryogenic separation and distillation theory. Energies 2014;7(5):3484–502.
[127] Ramdin M. CO_2 Capture with ionic liquids: experiments and molecular simulations. TU Delft: Delft University of Technology; 2015.
[128] Zhang X, et al. Carbon capture with ionic liquids: overview and progress. Energy Environ Sci 2012;5(5):6668–81.
[129] Kumełan J, Tuma D, Maurer G. Simultaneous solubility of carbon dioxide and hydrogen in the ionic liquid [hmim][Tf 2 N]: experimental results and correlation. Fluid Phase Equilibria 2011;311:9–16.
[130] Ramdin M, et al. Solubility of CO_2 and CH4 in ionic liquids: ideal CO_2/CH4 selectivity. Ind Eng Chem Res 2014;53(40):15427–35.
[131] Rosli A, et al. Advances in Liquid Absorbents for COˆ sub 2ˆ Capture: a Review. J Phys Sci 2017;28:121.
[132] Burr B, Lyddon L. A comparison of physical solvents for acid gas removal. In: Proceedings of the 87th annual gas processors association convention, Grapevine, TX, March.; 2008.
[133] Xie Y, et al. Energy consumption analysis for CO2 separation using imidazolium-based ionic liquids. Appl Energy 2014;136:325–35.
[134] Zhang Y, et al. Dual amino-functionalised phosphonium ionic liquids for CO_2 capture. Chem Eur J 2009;15(12):3003–11.
[135] Gurkan BE, et al. Equimolar CO_2 absorption by anion-functionalized ionic liquids. J Am Chem Soc 2010;132(7):2116–7.
[136] Bates ED, et al. CO_2 capture by a task-specific ionic liquid. J Am Chem Soc 2002;124(6):926–7.
[137] Zhang X, et al. Gas–liquid mass-transfer properties in CO_2 absorption system with ionic liquids. AIChE J 2014;60(8):2929–39.
[138] Bara JE, et al. Room-temperature ionic liquids and composite materials: platform technologies for CO_2 capture. Acc Chem Res 2009;43(1):152–9.
[139] Yang J, et al. CO_2 capture using amine solution mixed with ionic liquid. Ind Eng Chem Res 2014;53(7):2790–9.
[140] Zhao Y, et al. Density, viscosity, and performances of carbon dioxide capture in 16 absorbents of amine+ ionic liquid+ H2O, ionic liquid+ H2O, and amine+ H2O systems. J Chem Eng Data 2010;55(9):3513–9.
[141] Xu F, et al. Solubility of CO 2 in aqueous mixtures of monoethanolamine and dicyanamide-based ionic liquids. Fluid Phase Equilibria 2014;365:80–7.
[142] Shahrom M, Wilfred C. Synthesis and thermal properties of amino acids ionic liquids (AAILS). J Appl Sci 2014;14(10):1067.
[143] Fukumoto K, Yoshizawa M, Ohno H. Room temperature ionic liquids from 20 natural amino acids. J Am Chem Soc 2005;127(8):2398–9.
[144] Wang C, et al. Carbon dioxide capture by superbase-derived protic ionic liquids. Angew Chem 2010;122(34):6114–7.
[145] Ma C, et al. Development of low-cost deep eutectic solvents for CO2 capture. Energy Procedia 2017;142:3320–5.
[146] Adeyemi I, Abu-Zahra MR, Alnashef I. Novel green solvents for CO_2 capture. Energy Procedia 2017;114:2552–60.
[147] Arshad MW. CO_2 capture using Ionic Liquids. Lyngby, Denmark: Technical University of Denmark, DTU, DK-2800 Kgs; 2009.
[148] Sigma-Aldrich. 2017. Available from: 〈https://www.sigmaaldrich.com/〉.
[149] Hallett JP. Tuning ionic liquids for low cost: applications in lignocellulose deconstruction, In: Proceedings of the International Symposium on Tunable Solvents For Green Processing. InPROMPT 20162/3 June 2016 Berlin; 2016.
[150] Chen L, et al. Inexpensive ionic liquids: [hso 4] −-based solvent production at bulk scale. Green Chem 2014;16(6):3098–106.
[151] Zhai H, Rubin ES. Systems analysis of ionic liquids for post-combustion CO 2 capture at coal-fired power plants. Energy Procedia 2014;63:1321–8.
[152] Wappel D, et al. Ionic liquids for post-combustion CO2 absorption. Int J Greenh Gas Control 2010;4(3):486–94.
[153] Oliferenko AA, et al. Prediction of gas solubilities in ionic liquids. Phys Chem Chem Phys 2011;13(38):17262–72.
[154] Mortazavi-Manesh S, Satyro MA, Marriott RA. Screening ionic liquids as candidates for separation of acid gases: solubility of hydrogen sulfide, methane, and ethane. AIChE J 2013;59(8):2993–3005.
[155] Maiti A. Theoretical screening of ionic liquid solvents for carbon capture. ChemSusChem 2009;2(7):628–31.
[156] Sairi NA, et al. Low pressure solubilities of CO2 in guanidinium trifluoromethanesulfonate–MDEA systems. Fluid Phase Equilibria 2015;385:79–91.
[157] Ramdin M, de Loos TW, Vlugt TJH. State-of-the-Art of CO_2 Capture with Ionic Liquids. Ind Eng Chem Res 2012;51:8149–77.
[158] Maia FM, et al. Modeling of ionic liquid systems: phase equilibria and physical properties. Ionic Liquids-New Aspects for the Future. InTech; 2013. p. 31–60.
[159] Danesh A. PVT and phase behaviour of petroleum reservoir fluids. 47. Elsevier; 1998.
[160] Qi G, Wang Sh. Modeling solid-liquid equilibrium of the NH3-CO_2-SO2-K2SO4-H2O system and its application to combined capture of CO_2 and SO2 using aqueous ammonia. Energy Procedia 2017;114:834–9.
[161] Pearson P, Moscatelli J, Garg B, Cousins A, Feron PHM. An update on the development of the CSIRO's CS-Cap combined CO_2 and SO2 capture process. Energy Procedia 2017;114:1721–8.
[162] Luo M, Yi Y, Wang Sh, Wang Z, Wang Q. Review of hydrogen production using chemical-looping technology. Renew Sustain Energy Rev 2018;81(2):3186–214.
[163] Pires JCM. COP21: The algae opportunity? Renew Sustain Energy Rev 2017;79:867–77.
[164] Brynolf S, Taljegard M, Grahn M, Hansson J. Electrofuels for the transport sector: a review of production costs. Renew Sustain Energy Rev 2018;81(2):1887–905.